Shinohara, M., Salisbury, M.H., and Richter, C. (Eds.)
Proceedings of the Ocean Drilling Program, Scientific Results Volume 195

12. Analysis of NGR Spectra from Deep-Sea Sediments in the Philippine Sea, Site 1201[1]

S.M. Dean[2]

ABSTRACT

Natural gamma ray measurements are made routinely during core logging using the physical property multisensor track. The instrument provides a measure of the natural decay of radioactive elements in the core, expressed in counts per second, which is generally used as a proxy for the clay content of nonmarginal marine sediments. At Site 1201 spikes of increased gamma ray emissions, up to six times the average for the entire core over depth intervals on the order of 20–50 cm, are observed from the sediments within 50 m of the basement contact. The spikes show a strong correlation with sediment color variations, coinciding with red/brown layers within otherwise green/gray-colored sediments. In this paper, the gamma ray spectra obtained from 21 measurements using a 4-hr counting period are analyzed to obtain the absolute concentration of the radioactive elements K_2O, U, and Th in both the intervals with spikes and the intervals with relatively low count rates. In addition, the concentration of these elements is estimated using the spectra obtained from the routine 20-s counting period measurements and which, although exhibiting a great deal of scatter due to the high statistical uncertainty in the original measurements, are roughly similar to those obtained from the 4-hr counting period. Baseline concentrations for U (1 ppm) and Th (5 ppm) match published averages for the amount present in deep-sea clays; the peak concentrations measured correspond to an additional concentration of 100%–200%. The results are compared to those from downhole logging and shipboard inductively coupled plasma–atomic emission spectrometry measurements. The gamma ray spectra results do not support post-

[1]Dean, S.M., 2004. Analysis of NGR spectra from deep-sea sediments in the Philippine Sea, Site 1201. *In* Shinohara, M., Salisbury, M.H., and Richter, C. (Eds.), *Proc. ODP, Sci. Results,* 195, 1–33 [Online]. Available from World Wide Web: <http://www-odp.tamu.edu/publications/195_SR/VOLUME/CHAPTERS/105.PDF>. [Cited YYYY-MM-DD]
[2]Southampton Oceanography Centre, School of Ocean and Earth Science, University of Southampton, Waterfront Campus, European Way, Southampton SO14 3ZH, United Kingdom. **smd9@soc.soton.ac.uk**

Initial receipt: 19 January 2004
Acceptance: 23 August 2004
Web publication: 1 December 2004
Ms 195SR-105

depositional fluid flow through the sediment as the source of the enrichment of radioactive elements. It is more likely that the spikes in the gamma ray emissions are simply the result of interbedding sediments from two different sources, one with relatively high concentrations of K_2O, U, and Th.

INTRODUCTION

Unstable (radioactive) elements present in sediment and rock naturally decay over time. When such an element decays, alpha particles, beta particles, and/or gamma rays are emitted and a new isotope is formed as a decay product. Alpha and beta particles have relatively low energy and are not generally detected by logging equipment. Gamma rays have high energy and are detected. The main radioactive elements in the geological environment are potassium (^{40}K), uranium (^{238}U), and thorium (^{232}Th). The energy of a gamma ray is dependent on the element or isotope that is decaying. The decay product may also be unstable and decay further, emitting more gamma rays with different energies than those from the original element; each radioactive element therefore produces one or more characteristic decay lines. However, gamma ray emissions measured from rock samples are typically in the range of 300–3000 KeV where Compton scattering is dominant and, hence, the measured energy spectrum forms a continuous function with relatively broad peaks relating to the elemental decay lines present.

The natural gamma ray (NGR) detector used by the Ocean Drilling Program (ODP) comprises four doped sodium iodide scintillation counters and photomultiplier tubes in an orthogonal arrangement, where the core passes through the center (Hoppie et al., 1994). NGR measurements are made routinely as a part of the physical properties measured by multisensor track (MST) but only to provide a measure of the total counts per second (cps). In addition to counting decays, the NGR detector also determines the energy of each gamma ray emission in 1 of 256 energy windows between 0 and 3000 KeV. Blum et al. (1997) outline a method for using the NGR spectra to calculate the relative abundance of the radioactive elements in the sample. Their method involves integrating the area under certain peaks in the NGR spectrum and deriving empirical formulas relating the NGR results to laboratory analyses (i.e., X-ray fluorescence, inductively coupled plasma–mass spectrometry [ICP-MS], and instrument neutron activation analysis [INAA]) on crushed samples of the cores on which the NGR measurements were made.

This study looks at the NGR spectra from measurements made on the deepest sediments at Site 1201 and applies the method of Blum et al. (1997) to determine radioactive element concentrations. A 509-m sedimentary section, composed of an upper and lower unit, was cored at Site 1201. The lower unit, from 53 meters below seafloor (mbsf) to the basement at 509 mbsf, consists of late Oligocene to late Eocene interbedded turbidites that are pervasively green-gray in color. Toward the bottom of the lower unit, laminations in the turbidites on the order of 5 cm and thicker are observed with a distinct reddish brown color, and the basal 2.5 m is composed of a brown claystone. During the routine MST logging of the core at Site 1201, the average NGR measurement was ~5 cps; however, spikes of as high as 30 cps were observed in the sediments within 50 m of basement. Radioactive element concentra-

tion measurements can help determine the mineralogy and abundance of clay and other radioactive minerals including micas and feldspars (Serra, 1998). They can also help characterize depositional environment and diagenetic processes in sediments (Blum et al., 1997). The spikes in the NGR appeared to coincide with the red-brown sediment; these were the intervals chosen for a more detailed study.

METHODS

Data Acquisition

The routine counting period for an NGR measurement during Leg 195 was 20 s. Even with a peak emission rate of 30 cps, such a relatively short counting period results in an energy spectrum with a large statistical uncertainty in each energy window. To overcome this, the counting period must be significantly increased, but this is impractical during the majority of ODP legs where core is rapidly recovered and must be passed through the MST. The science program for Site 1201 required a significant amount of time to be spent on the emplacement of a downhole International Ocean Network seismometer after normal coring operations were complete. The MST was available during the operation to install the seismometer, allowing NGR measurements to be made over 4-hr counting periods at 21 locations in the sediments. Because these measurements could only be made after normal ODP operations at the site were complete, they were performed on the archive half of the split core. All measurements, including the depth intervals at which they were made, are given in Table **T1;** this includes two measurements of the background spectrum. Example spectra to compare the results of a 4-hr counting period to that obtained during the routine ODP core logging are shown in Figure **F1.**

T1. Raw NGR emissions, Site 1201, p. 20.

F1. NGR spectrum comparison, p. 11.

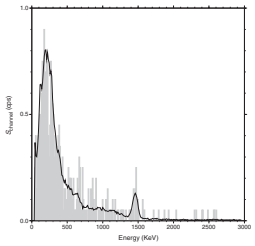

Data Processing and Analysis

Following Blum et al. (1997), the NGR spectra are processed and analyzed in the following steps:

1. Calibrate NGR energy windows.
2. Remove background spectrum.
3. Correct for missing core volume.
4. Filter (3-point mean boxcar).
5. Integrate counts within energy intervals containing peak NGR emissions.

The energy of an NGR emission is measured on the MST in 256 discrete levels, or energy windows, that were calibrated at the start of Leg 195 using sources of potassium (^{40}K) and thallium (^{208}Tl). Calibration results are given in Table **T2.** The mean energy attributed to the center of window number W_x (0–255), calibrated in kiloelectron volts, is defined in Equation 1, and the width of each window is 11.79 KeV.

T2. NGR calibration results, p. 32.

$$\text{Mean window energy (KeV)} = 11.79W_x + 33.93. \quad (1)$$

The background spectrum is a measure of the gamma ray energy that enters the NGR instrument and that does not originate from the core sample. This should mainly be cosmic radiation. The background spec-

trum must be removed from each core measurement, but determining a sensible spectrum proved not to be trivial, and a number of test counts were made with the NGR instrument empty or containing an empty core liner or a core liner full of deionized water. Spectra obtained from measurements on an empty core liner or with the NGR instrument empty have an overall higher count rate than those obtained when a water-filled core liner was inserted into the NGR. For background counts other than those obtained when the NGR instrument contains a water-filled core liner, the counts in some energy windows >2000 KeV exceed the raw counts obtained when a core sample is inserted in the NGR. There is little difference between the background spectra with the NGR empty or with an empty core liner, and if either are used to correct the NGR data then the total corrected count obtained from each 4-hr measurement is ~10% less than that obtained from the 20-s counting period at the same depth interval. However, if instead the spectrum obtained from the water-filled core liner is used as the background, the total count (cps) obtained from the 4-hr period is ~15% greater than that obtained from the 20-s count period. It seems likely that a sample placed in the NGR acts to block gamma rays from external sources from entering the instrument; because the 4-hr measurements were made on the split core, the NGR sample space was effectively half full and so the optimal background count lies somewhere between those obtained with the NGR empty and those with a water-filled core liner. The background spectrum chosen to correct all the data was taken to be the mean of these counts (Fig. **F2**). An example NGR spectrum after the background has been removed and the application of a three-point mean boxcar filter is shown in Figure **F3.**

A volumetric correction is applied to account for a smaller than normal core diameter obtained in Hole 1201D by rotary core barrel (RCB) coring and for the 4-hr measurements being made on the archive half of the split core. The good recovery at Site 1201 meant that there was no need to apply a correction for void spaces in the core (e.g., Lyle et al., 1996); any gaps or highly fractured sections of core were avoided in making the 4-hr measurements. The average core diameter recovered from the RCB cores at Site 1201 was ~5.75 cm instead of the nominal 6.6 cm. Equation 2 gives the total volumetric correction, where S is the number of counts.

$$S_{\text{volumetric}} = 2(6.6^2/5.75^2)S_{\text{measured}}. \quad (2)$$

Blum et al. (1997) split the NGR spectrum into 16 energy intervals (S_{I1}–S_{I16}), each containing one or more discrete peak in the number of counts (Fig. **F3**). They then define the peak baseline as the line that passes through the local minima that bound each energy interval (Fig. **F4**). The integrated counts above the peak baseline (S_P) and below the peak baseline (S_B), for selected peaks in the energy spectrum, form the basis of Blum et al.'s element concentration analysis. They recommend using the integrated counts in the peak area of interval six (S_{P6}; ~1330–1580 KeV) and the background-corrected total count rate (S_{TC}) for the analysis. K_2O concentration in weight percent is linearly related to S_{P6} (Eq. 3); U and Th concentrations in parts per million are linearly related to S_{TC} (Eqs. 4 and 5).

$$x'_K = 0.506 + 1.43S_{P6} \pm \{16 + [0.67 \times \text{SQR}(S)/S]100\}\%, \quad (3)$$

F2. Background spectrum counts, p. 12.

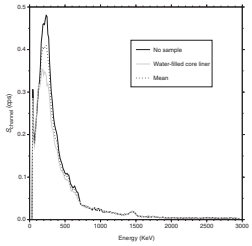

F3. NGR spectra for 509.36 mbsf, p. 13.

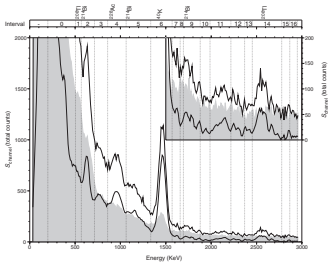

F4. Peak baseline definition, p. 14.

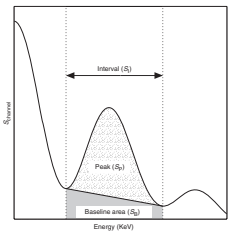

$$x'_U = 0.279 + 0.0762S_{TC} \pm \{30 + [0.67 \times SQR(S)/S]100\}\%, \text{ and} \quad (4)$$

$$x'_{Th} = 1.66 + 0.389S_{TC} \pm \{20 + [0.67 \times SQR(S)/S]100\}\%. \quad (5)$$

With a small modification, the above method can be directly applied to the NGR data obtained from the routine 20-s counting period data, for the purpose of comparison. Although there is an increased uncertainty in the results, Hoppie et al. (1994) show that S_{TC} measured with a 20-s count period for sediments with a similar level of gamma ray activity has a relatively low standard deviation of 7.4%, only reducing to <5% for significantly longer counting periods. K_2O is more difficult to determine because, as shown in Figure **F1,** S_{P6} is hard to determine when the local minima in the spectrum are so poorly defined. One possible compromise solution is to see if there is any relationship between S_{P6} and the total counts in interval six (S_{I6}), which is easy to calculate, and then use S_{I6} to determine the concentration of K_2O. When S_{P6} is plotted against S_{I6}, both calculated from the 4-hr counting period data, a trend appears (Fig. **F5**). The best-fit straight line to this data, which also passes through the origin, is given in Equation 6.

F5. S_{I6} vs. S_{P6}, p. 15.

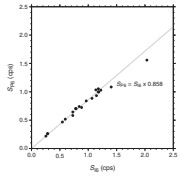

$$S_{P6} = S_{I6} \times 0.858. \quad (6)$$

The K_2O concentration for the 20-s counting period NGR data can then be determined using Equation 7.

$$x'_K = 0.506 + 1.23S_{I6} \quad (7)$$

DISCUSSION

The final corrected gamma ray spectra are shown in Figure **F6.** A number of general observations can be made.

F6. NGR total count, a*, and gamma ray spectra, p. 16.

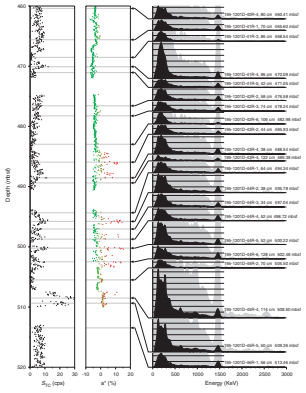

1. The highest peak counts occur at 508.50 and 509.36 mbsf, both intervals in the brown claystone that also have the highest total count peaks by a significant margin, and at 470.09 mbsf, in the turbidites above the section of red-brown laminations, but without a significantly higher total count peak.
2. The lowest peak counts occur at 468.54, 471.05, 489.38, 494.34, and 505.50 mbsf, depth intervals chosen for 4-hr counts specifically because they were observed to have a low total count during routine core logging, to provide a baseline measure of the element concentration.
3. The spectrum at 513.46 mbsf, the only measurement in the basalt, does not appear to be very different from those made in the overlying sediment.

To make a detailed discussion of the spectra, the energy spectrum will be considered in two parts, a low- and high-energy region.

The region below 500 KeV contains lower-energy thorium and uranium emissions but has a large component of emissions that have been affected by Compton scattering in the sample. The main emission peak in this region is composed of at least four smaller, second-order peaks at 120, 190, 275, and 400 KeV. The sizes of these peaks vary downsection, particularly the relative size of the 190-KeV peak vs. both the 120- and

275-KeV peaks (Fig. F7). The 120- and 275-KeV peaks are prominent and larger than the 190-KeV peak in the majority of the spectra, especially those at 508.50 and 509.36 mbsf. In the spectra at 468.54, 470.09, 482.98, and 505.50 mbsf, the central 190-KeV peak becomes more prominent and merges with the 120-KeV peak. The spectrum at 470.09 mbsf is of particular note in that it has the second highest peak count and corresponds to a relatively high total count of 12 cps; it appears anomalous located above the section of red-brown laminations where the total counts are otherwise generally low. When the cumulative total counts are calculated as a function of increasing energy (Fig. F8), the curves plot in two clusters that correspond to the pattern of peaks observed in the low-energy region. Spectra with prominent peaks at 120 and 275 KeV correspond to a cumulative count that plots lower for a given energy than when the 190-KeV peak is prominent. In other words, where spectral peaks at 120 and 275 KeV are prominent, there is a relative increase in the gamma ray emissions toward the higher end of the energy spectrum. Although the low-energy region accounts for ~75% of the total gamma ray emissions, Blum et al. (1997) analyze it as a single interval, thus making it unclear whether the observed trend is related to the presence of any particular element.

The high-energy region above 500 KeV contains many discrete emission peaks that can be identified. The most prominent peak in this region is that for ^{40}K at 1460 KeV, but other peaks can also be identified: ^{214}Bi, particularly at 609 KeV, from the uranium decay series and ^{208}Tl at 2615 KeV and ^{228}Ac at 911–969 KeV from the thorium decay series. The ^{40}K peak directly relates to the total potassium concentration, which will be discussed in the next section. The other peaks in the high-energy region are more variable, and it is difficult to identify any obvious patterns downsection from the spectra alone.

The concentrations of K_2O, U, and Th calculated from the 4-hr counting period measurements are given in Table T3. K_2O varies between 0.82 and 2.74 wt% (mean = 1.61 wt%). U varies between 0.61 and 2.95 ppm (mean = 1.17 ppm). Th varies between 3.35 and 15.29 ppm (mean = 6.23 ppm). Ignoring all the measurements at NGR peaks, the baseline concentration in this interval is 1.28 wt% for K_2O, 0.84 ppm for U, and 4.50 ppm for Th. The highest concentration for each element is measured in the brown claystone at a depth of ~508.50 mbsf. There is ~200% more U and Th in the brown claystone relative to the gray-green sediments, whereas there is only ~150% more K_2O. The red-brown laminations have a more modest increase of ~50% U and Th but ~100% for K_2O. The results obtained from both the 4-hr and 20-s counting periods are plotted in Figure F9 and compare favorably, especially for U and Th. In general, the element concentrations obtained from the 20-s count period NGR data are lower than those from the 4-hr counting period data. This result is not unexpected since most of the 4-hr measurements were specifically made over depth intervals where local peaks in the total counts were identified. Unsurprisingly, there is considerably greater scatter in the results from the short-period measurements. However, for U and Th, most of the 20-s values lie within the error bars of the 4-hr values. By comparison, K_2O concentration, estimated from the 20-s counting period, exhibits far greater scatter (in excess of 50% of the mean value). The larger scatter in K_2O concentration is a consequence of being calculated from counts from only a fraction of the full energy spectrum, which increases the uncertainty in the number of counts measured. The S_{I6} energy window used to calculate

F7. Brown claystone, green-gray sediment, and basalt basement NGR spectra, p. 17.

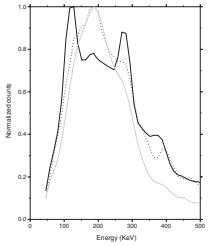

F8. All NGR spectral measurements at Site 1201, p. 18.

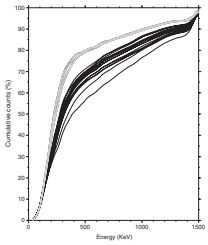

T3. K_2O, U, and Th concentrations, p. 33.

F9. K_2O, U, and Th concentrations, p. 19.

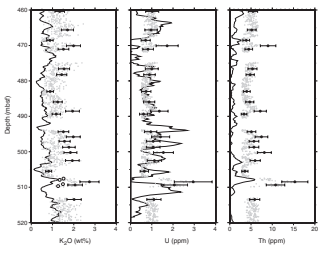

K_2O concentration contains <10% of the total counts used for the other elements (Fig. F8).

Geochemical analyses at Site 1201 included six shipboard inductively coupled plasma–atomic emission spectrometer (ICP-AES) measurements for K_2O in the brown claystone between 507.56 and 509.7 mbsf. The ICP-AES values vary from 1.05 to 1.52 wt% (mean = 1.31 wt%), which makes them fall within the scatter of the concentrations from the 20-s measurements but outside of the error bars from the 4-hr measurements (Fig. F9). The geochemical analysis locations do not exactly match the depth intervals for any of the 4-hr measurements, so it is possible that the very active layers in the NGR data are as thin as a few centimeters, which would be below the resolution of the NGR instrument (Hoppie et al., 1994). Downhole measurements with the Schlumberger logging tool also provide the concentration of K_2O, U, and Th, and these are shown in Figure F9. Initially there appears to be little similarity between the data sets. However, the relative variations in concentrations of K_2O and Th downsection are similar; the major peak over the brown claystone is also present in the downhole data, and other smaller peaks (e.g., at 53 mbsf) are clear in both data sets. However, the downhole concentrations are 0.5–1.0 wt% lower for K_2O and as much as 5 ppm for Th. The downhole concentration of U has a similar mean value of ~1 ppm but exhibits considerably greater variation than the NGR results and, for the brown claystone in particular, often shows a decrease in concentration where the NGR results show an increase. The reason for this discrepancy is not clear. The average concentrations of K_2O, U, and Th in deep-sea sediment are 2.1 wt%, 1 ppm, and 5 ppm, respectively (Chester and Aston, 1976), very similar to the mean values determined from the NGR measurements but also similar to the peak values measured by downhole logging in the brown claystone that may be the most appropriate lithology with which to compare the published values. The ICP-AES measurements of K_2O concentration do not corroborate either the concentrations from the downhole logging or the NGR because they lie between the two results.

The increased concentrations of K_2O, U, and Th in the red-brown sediments could be related to either a change in the sediment source, the depositional environment, or the diagenesis of the sediments. One possibility is that the high element concentrations have been affected by fluid flow through the sediments. However, the relative mobility of each radioactive element is different (in particular, uranium is soluble whereas thorium is not) but in the Site 1201 results, the ratio of U to Th concentration changes very little between regions with high and low total counts. Another possibility is that the NGR results simply reflect the interbedding of the brown claystone with high NGR emissions and the turbidites that have otherwise relatively low NGR emissions, resulting in the red-brown colored sections. The source of the brown claystone appears to only have been active during the early stages of the deposition of the sequence. This interpretation is consistent with the lithostratigraphic descriptions of the core. However, the proportionate increase in the concentration of K_2O, U, and Th is not the same in the claystone as in the red-brown sediment, nor does this explain the high emissions at 470.09 mbsf, where the red-brown coloration is absent.

The similarity observed between the element concentrations determined from 4-hr and 20-s counting period spectra have a number of consequences. First, the element composition could be determined where only short count period data are available (e.g., existing ODP

NGR data) to provide a rough estimate of the radioactive element composition at other sites. Although speculative, it may also suggest that the current analysis technique is not extracting all possible information from the 4-hr spectra, which clearly have a much-improved resolution of the spectral peaks. It may be worthwhile to investigate the sensitivity of the NGR to a number of key decay products in the U and Th series to develop the analysis using multiple spectral peaks together to provide the total element concentration. Blum et al. (1997) show that, with the exception of a K peak at 1460 KeV (S_{P6}), a single spectral peak does not statistically relate to the total concentration of any parent element. In analyzing the downhole spectral NGR data, Schlumberger splits the gamma ray spectrum in a relatively simple way, into five energy windows (Schlumberger, 1987). However, through the calibration of the instrument using a number of sources with known element concentrations, the instrument can calculate the total element concentration in any other sample using a function that weights the counts in each window. The ODP instrument, with 256 energy windows that can be combined to target spectral peaks relating to a single decay product (such as those defined by Blum et al. [1997]), could be calibrated to either replicate the Schlumberger results or, more usefully, give the relative abundance of the decay products for each element.

CONCLUSIONS

The analysis of spectral NGR data acquired by the MST at Site 1201 shows the following:

1. Baseline concentrations for U (~1 ppm) and Th (~5 ppm) in the sediments match published averages for deep-sea sediment. The measured concentration of K_2O is generally less than the published average of 2.1 wt%. The concentration of K_2O in the Site 1201 sediments below 460 mbsf is generally very low. Shipboard K_2O concentration measurements by ICP-AES are even lower than those derived from the NGR spectra.
2. Peak concentrations of K_2O, U, and Th in the red-brown layers of the sediment are ~100% above those in the adjacent gray-green sediments; concentrations in the brown claystone layers at the basement contact are elevated by 100%–200% relative to the gray-green sediments.
3. Analysis of the low-energy region (<500 KeV) identifies clear trends in the spectrum that may be related to the concentration of specific elements but cannot be determined by the current analysis method.
4. The most likely source of the increased K_2O, U, and Th concentrations in the brown claystone and red-brown layers is a change in the composition of the sediment source rather than diagenetic alteration of the sediments. If fluid flow were affecting the radioactive element concentrations in specific layers, the U/Th ratio should vary with depth through the section, but this is not observed in the Site 1201 data.
5. Element concentrations determined from 4-hr and 20-s counting periods compare closely, although, unsurprisingly, the greater uncertainty in the shorter-period measurements gives more scatter in the results.

6. Comparison between the NGR element concentrations and those measured by downhole logging shows that the two techniques are not well calibrated. This is a major problem, and integrating the data sets would be especially useful because the downhole logging results could fill in gaps in the MST log where recovery was <100%.

ACKNOWLEDGMENTS

This research used data provided by the Ocean Drilling Program (ODP). ODP is sponsored by the U.S. National Science Foundation (NSF) and participating countries under management of Joint Oceanographic Institutions (JOI), Inc. Funding for this research was provided by the National Environment Research Council (United Kingdom) and Southampton Oceanography Centre. The author would like to thank Philippe Gaillot for his help with the downhole NGR data.

REFERENCES

Blum, P., 1997. Physical properties handbook: a guide to the shipboard measurement of physical properties of deep-sea cores. *ODP Tech. Note,* 26 [Online]. Available from World Wide Web: <http://www-odp.tamu.edu/publications/tnotes/tn26/INDEX.HTM>. [Cited 2003-10-15]

Blum, P., Rabaute, A., Gaudon, P., and Allan, J.F., 1997. Analysis of natural gamma-ray spectra obtained from sediment cores with the shipboard scintillation detector of the Ocean Drilling Program: example from Leg 156. *In* Shipley, T.H., Ogawa, Y., Blum, P., and Bahr, J.M. (Eds.), *Proc. ODP, Sci. Results,* 156: College Station, TX (Ocean Drilling Program), 183–195.

Chester, R., and Aston, S.R., 1976. The geochemistry of deep-sea sediments. *In* Riley, J.P., and Chester, R. (Eds.), *Chemical Oceanography* (2nd ed.): New York (Academic Press).

Hoppie, B.W., Blum, P., and the Shipboard Scientific Party, 1994. Natural gamma-ray measurements on ODP cores: introduction to procedures with examples from Leg 150. *In* Mountain, G.S., Miller, K.G., Blum, P., et al., *Proc. ODP, Init. Repts.,* 150: College Station, TX (Ocean Drilling Program), 51–59.

Lyle, M., Bristow, J., Bloemendal, J., and Rack, F.R., 1996. Comparison of natural gamma ray activity profiles from downhole logging and the MST core logger at Site 911 (Yermak Plateau). *In* Thiede, J., Myhre, A.M., Firth, J.V., Johnson, G.L., and Ruddiman, W.F. (Eds.), *Proc. ODP, Sci. Results,* 151: College Station, TX (Ocean Drilling Program), 369–376.

Schlumberger, 1987. *Log Interpretation Principles/Applications:* Houston (Schlumberger).

Serra, O., 1998. Role of well-logging in the study of sedimentary basins. In *Dynamics and Methods of Study of Sedimentary Basins:* New Delhi (Assoc. French Sedimentol.).

Figure F1. A comparison between the NGR spectrums obtained from a 4-hr counting period (black line; 488.54 mbsf) and a 20-s counting period (gray bars; 488.56 mbsf) used during the routing of MST core logging at Site 1201. Background counts have not been removed and the data are unfiltered, but the 4-hr measurements have been corrected for missing core volume (see text for details).

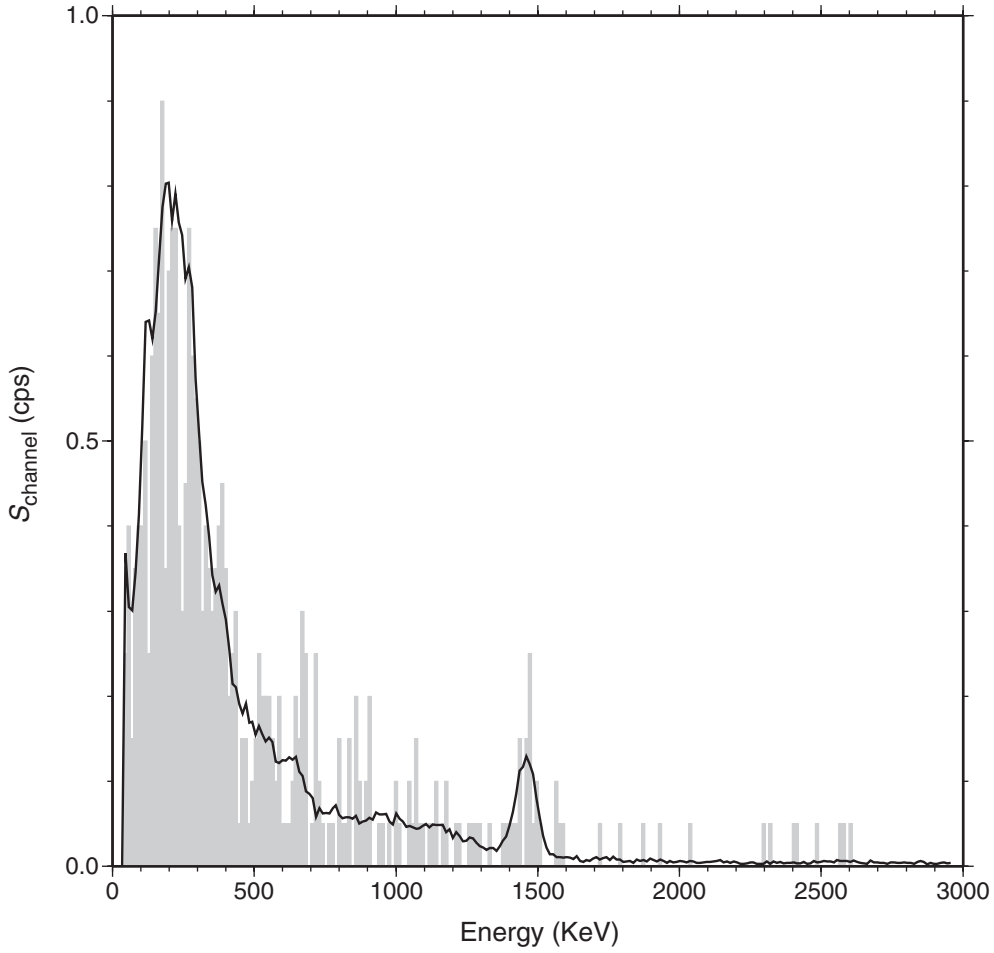

Figure F2. Counts of the background spectrum with the NGR instrument empty and containing a core liner filled with purified water.

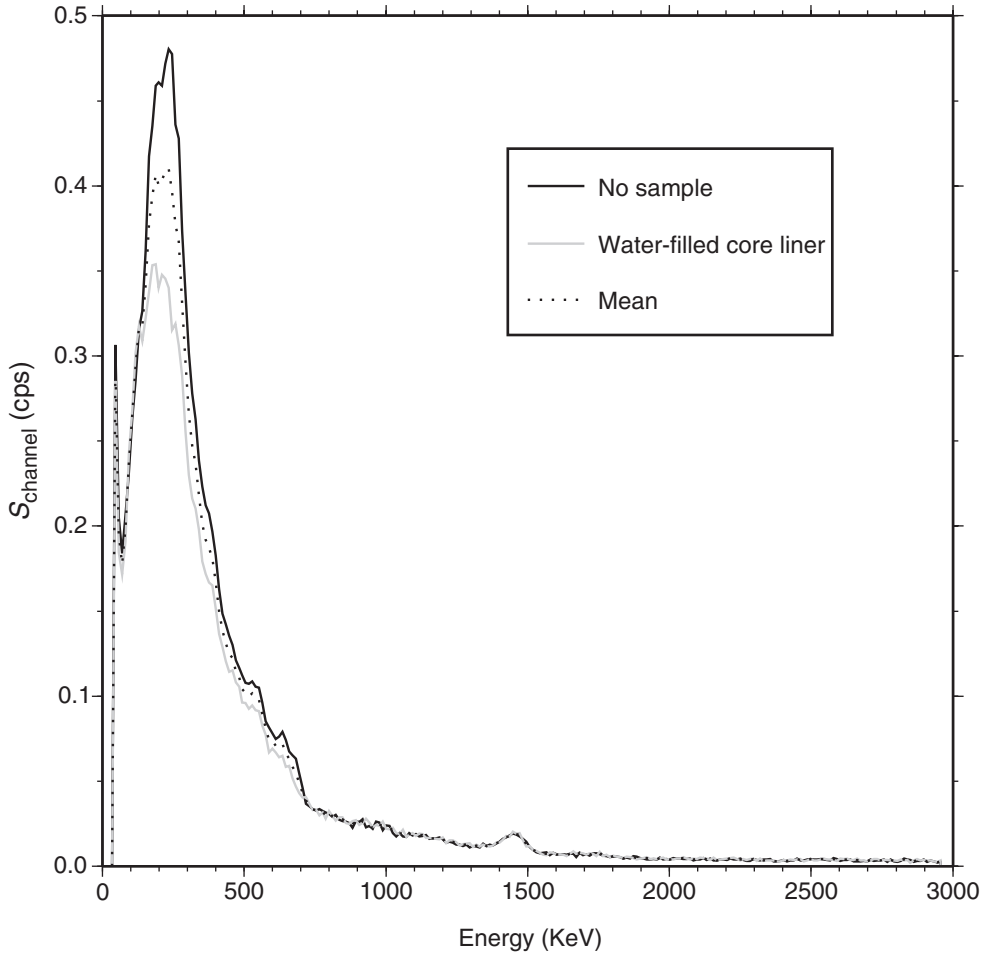

Figure F3. The NGR spectra for the measurement at 509.36 mbsf (heavy black line) after removing the background spectrum (gray region) and applying a three-point mean boxcar filter. The thin black line shows the raw spectrum. Dotted lines mark the interval boundaries defined by Blum et al. (1997). Prominent energy peaks relating to certain elements are identified at the top of the figure. The inset shows the spectrum for energies >1500 KeV at a 5× expanded scale.

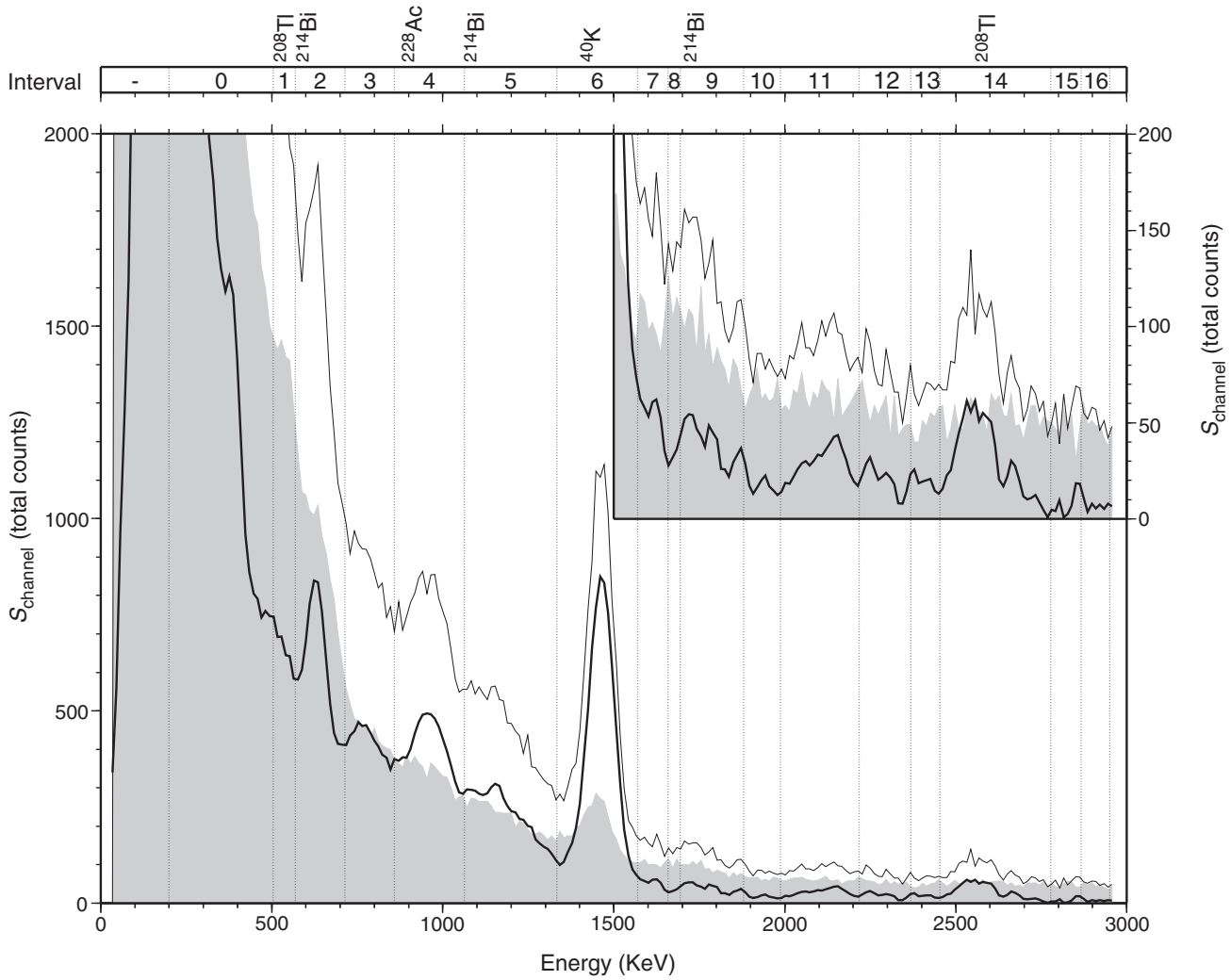

Figure F4. Definition of the peak baseline in NGR energy spectra (after Blum et al., 1997).

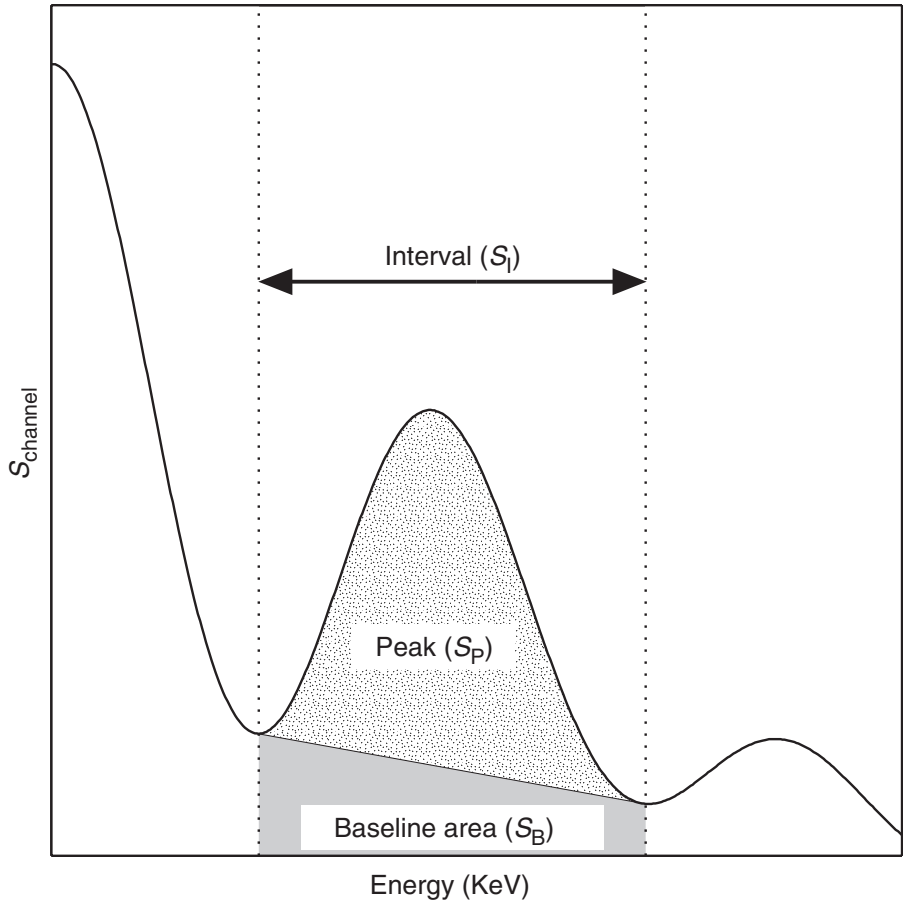

Figure F5. Plot of the total integrated counts within the peak area of interval six (S_{I6}) against only those above the baseline (S_{P6}) shows a simple linear relationship.

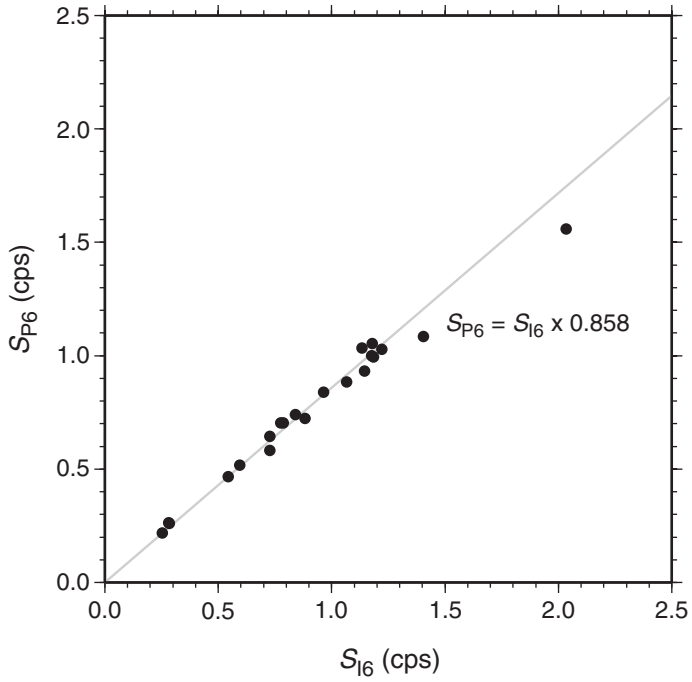

Figure F6. NGR total count measurements from routine core logging (left), a* (green-red, higher values being more red) chromaticity variable (Blum, 1997) (center), and gamma ray spectra (right). Each spectrum has been processed as described in the text. All spectra are plotted at the same vertical scale; gray spectra plotted at 10× vertical scale.

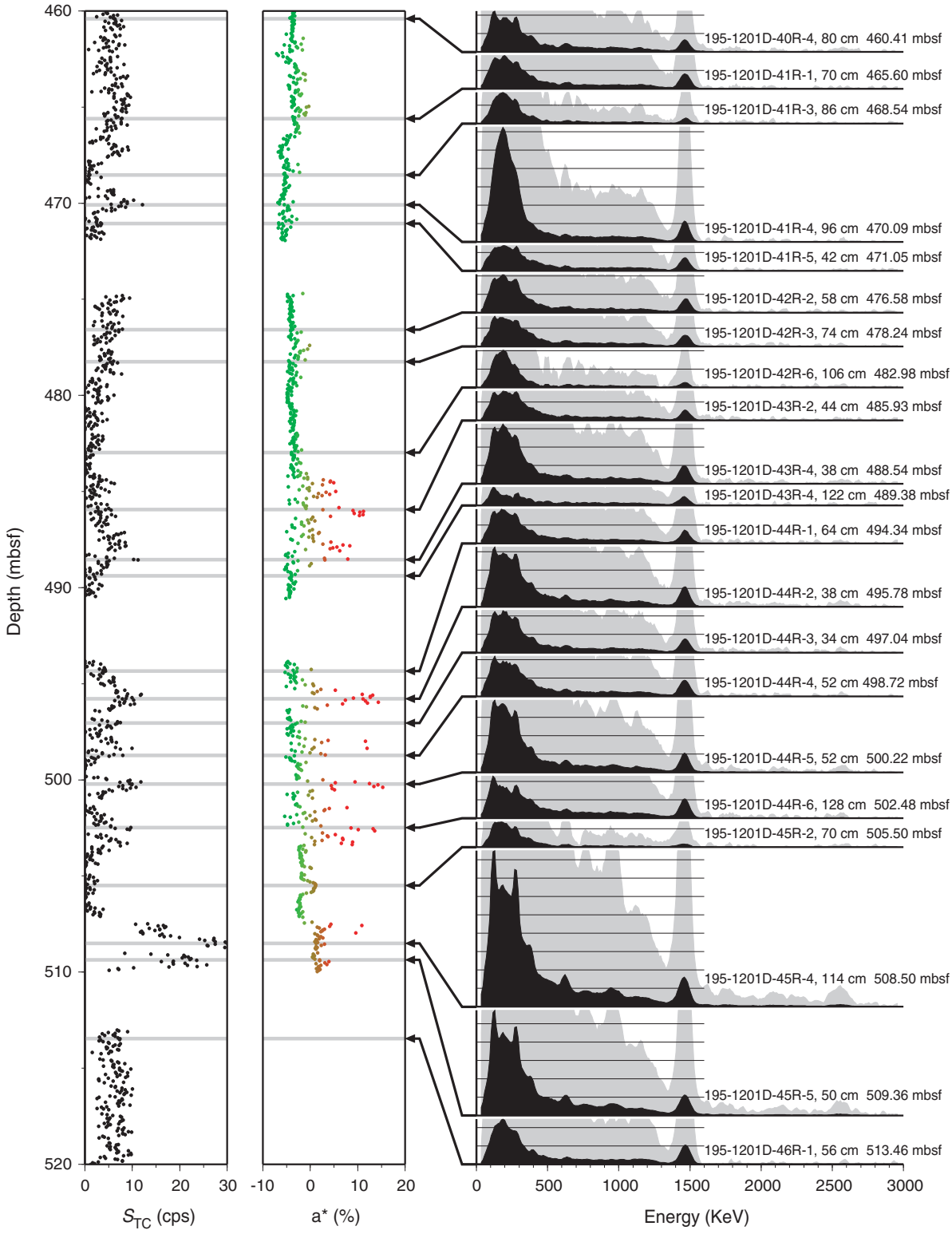

Figure F7. NGR spectra for measurements in brown claystone (black line, 508.50 mbsf), green-gray sediment (gray line, 470.09 mbsf), and basalt basement (dotted line, 513.46 mbsf), each normalized to the peak count. Although the spectrum at 470.09 mbsf is not typical of all the measurements in the gray-green sediment, this graph shows how peaks vary in the low-energy region of the gamma ray spectrum.

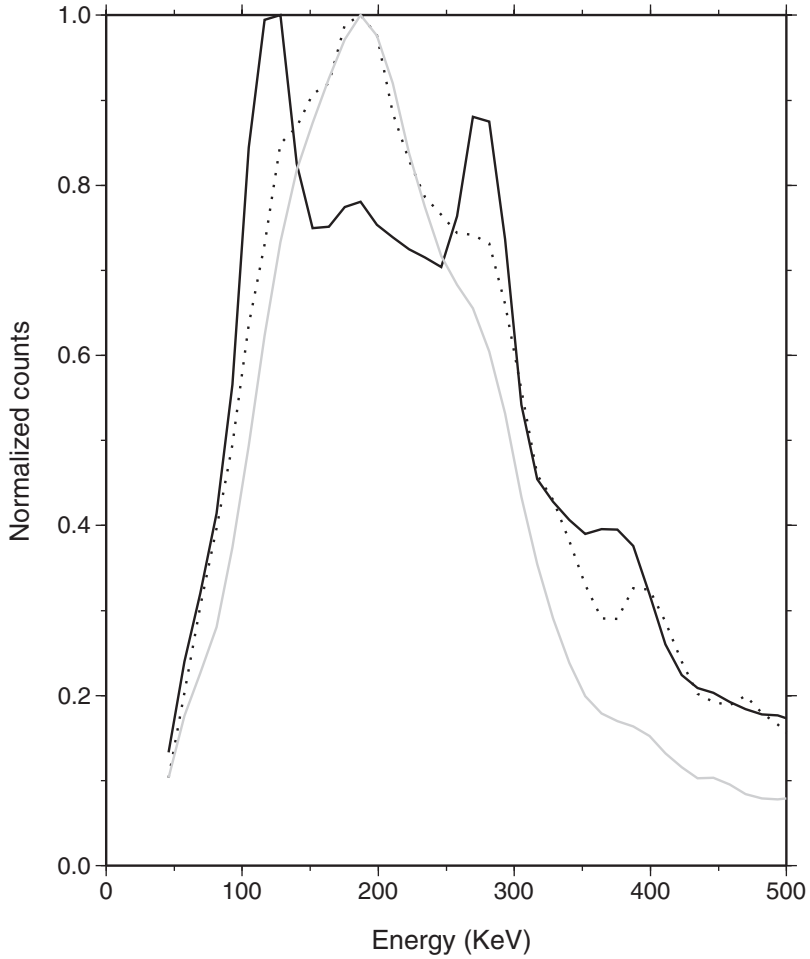

Figure F8. Cumulative counts with increasing energy for all NGR spectral measurements at Site 1201. Gray lines = measurements at 468.54, 470.09, 482.98, and 505.50 mbsf.

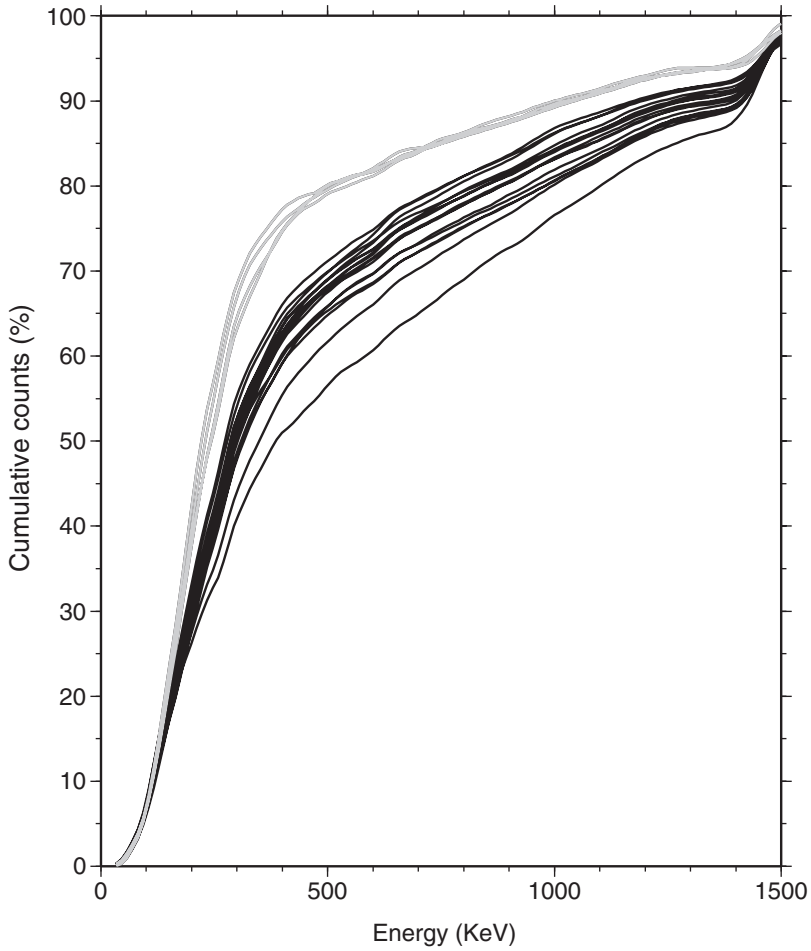

Figure F9. Concentrations of K_2O, U, and Th calculated from NGR measurements taken over a 4-hr counting period (black points with error bars), estimated from the routine 20-s counting period (gray points), and measured by downhole logging (black line). Open circles show shipboard ICP-AES measurements of K_2O concentration.

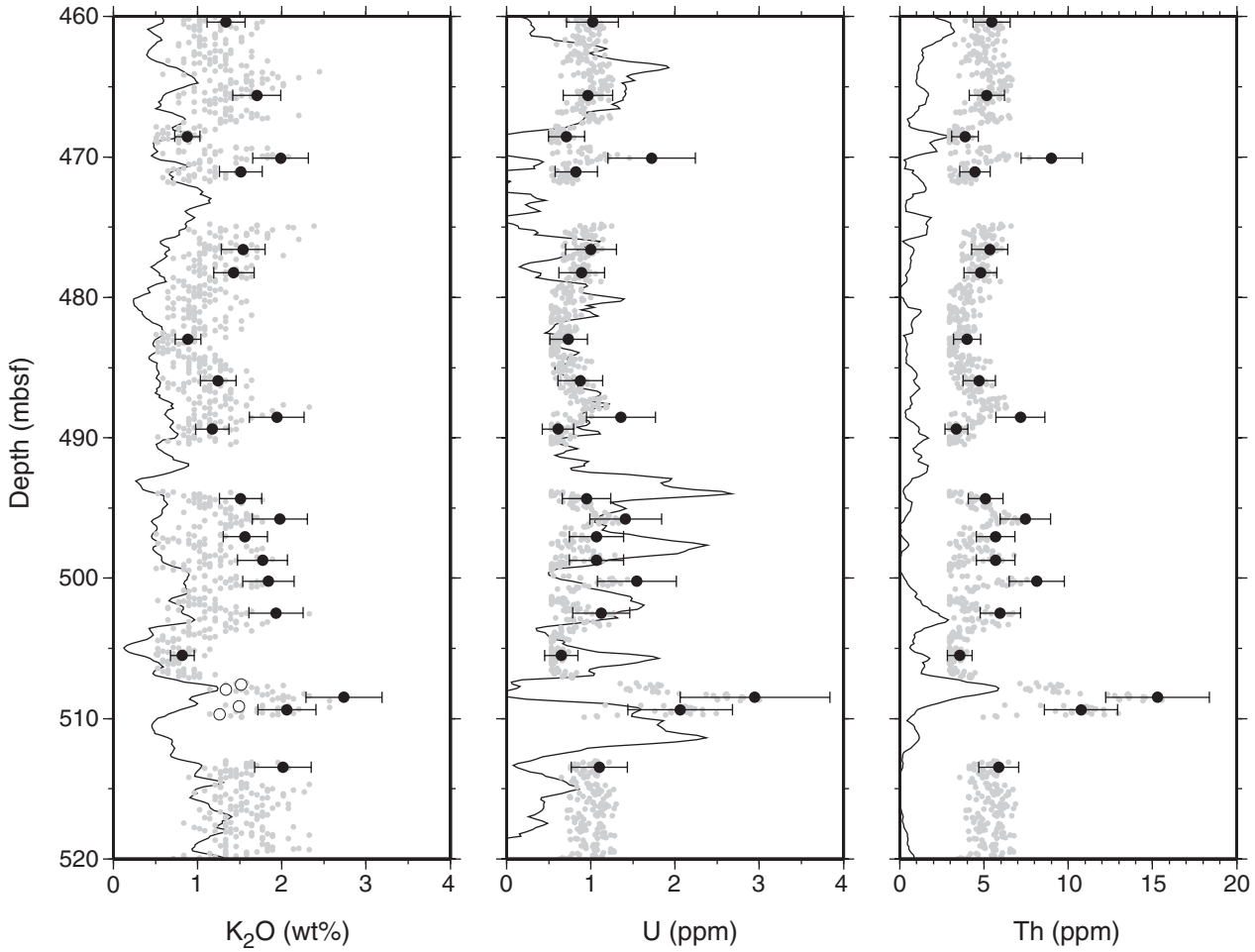

Table T1. Raw natural gamma ray emissions detected over a 4-hr counting period, Site 1201D. (**See table notes.** Continued on next 11 pages.)

Channel	Core, section, interval (cm): Mean energy (KeV)	195-1201D- 40R-4, 80	41R-1, 70	41R-3, 86	41R-4, 96	41R-5, 42	42R-2, 58	42R-3, 74	42R-6, 106	43R-2, 44	43R-4, 38	43R-4, 122	Empty	Water
0	33.93	0	2	2	0	1	2	2	2	2	1	2	5	3
1	45.71	4,624	4,513	4,383	4,848	4,366	4,483	4,505	4,402	4,390	4,704	4,286	4,413	4,110
2	57.50	3,285	3,193	3,092	3,689	3,248	3,170	3,193	3,080	3,091	3,525	3,024	2,955	2,657
3	69.29	3,130	3,086	2,795	3,594	3,080	3,153	3,089	2,918	3,060	3,400	2,737	2,648	2,470
4	81.07	3,654	3,616	3,261	4,156	3,355	3,646	3,250	3,241	3,410	3,866	3,187	2,970	2,750
5	92.86	4,325	4,169	3,898	5,065	4,074	4,272	4,136	4,030	3,972	4,722	3,778	3,329	3,489
6	104.64	5,251	4,853	4,582	6,181	4,541	4,979	4,656	4,588	4,744	5,651	4,491	3,782	3,851
7	116.43	6,118	5,491	5,148	7,219	5,143	5,783	5,629	5,421	5,495	6,780	5,057	4,113	4,346
8	128.21	6,190	5,812	5,658	8,054	5,539	5,941	5,792	5,863	5,750	6,909	5,284	4,544	4,573
9	140.00	6,112	5,920	5,625	8,495	5,560	5,899	5,673	5,866	5,567	6,690	5,199	4,699	4,447
10	151.79	6,195	6,094	6,115	9,120	5,817	6,280	6,032	6,425	5,950	7,020	5,419	5,209	4,643
11	163.57	6,701	6,570	6,666	9,717	6,489	6,959	6,583	6,739	6,472	7,581	6,011	6,012	4,860
12	175.36	7,002	6,915	6,971	10,345	6,659	7,111	7,029	7,178	6,822	8,125	6,027	6,267	5,088
13	187.14	7,197	7,217	7,102	10,695	6,845	7,499	6,950	7,433	7,071	8,329	6,216	6,610	5,096
14	198.93	7,332	7,224	7,070	10,455	6,899	7,407	6,915	7,304	7,014	8,234	6,284	6,635	4,896
15	210.71	7,124	7,102	7,003	10,133	6,803	7,165	6,991	7,246	6,929	7,970	6,164	6,609	5,005
16	222.50	7,235	7,048	7,017	9,932	6,803	7,186	6,953	7,276	7,064	8,182	6,337	6,795	4,973
17	234.29	7,240	7,120	6,970	9,425	6,924	7,149	6,986	6,847	7,005	7,897	6,289	6,918	4,896
18	246.07	6,836	6,799	6,658	9,136	6,644	7,034	6,845	6,754	6,838	7,616	6,021	6,875	4,541
19	257.86	6,561	6,441	6,367	8,665	6,194	6,702	6,371	6,353	6,422	7,269	5,769	6,279	4,593
20	269.64	6,632	6,246	6,200	8,329	6,164	6,661	6,217	6,102	6,344	7,279	5,494	6,163	4,411
21	281.43	6,507	6,095	5,978	7,799	5,954	6,259	6,145	5,937	6,202	6,977	5,565	5,376	4,152
22	293.21	5,494	5,320	5,016	6,774	5,237	5,522	5,189	4,858	5,327	5,973	4,730	4,850	3,684
23	305.00	4,657	4,680	4,390	5,834	4,450	4,715	4,654	4,381	4,598	5,337	4,108	4,349	3,311
24	316.79	4,349	4,347	3,991	5,202	4,218	4,358	4,303	4,077	4,390	4,811	3,896	4,002	3,115
25	328.57	4,125	4,137	3,795	4,795	4,044	4,161	3,981	3,858	4,160	4,574	3,790	3,785	3,028
26	340.36	3,946	3,921	3,562	4,240	3,675	3,866	4,002	3,516	3,763	4,226	3,414	3,434	2,850
27	352.14	3,522	3,606	3,279	3,791	3,447	3,525	3,539	3,167	3,547	3,754	3,170	3,213	2,579
28	363.93	3,346	3,283	2,975	3,599	3,055	3,304	3,343	3,007	3,286	3,560	2,995	3,057	2,473
29	375.71	3,428	3,237	3,023	3,509	3,200	3,243	3,198	2,950	3,153	3,580	3,026	2,988	2,402
30	387.50	3,292	3,125	2,921	3,373	3,023	3,167	3,206	2,933	3,198	3,413	2,888	2,833	2,379
31	399.29	3,000	2,982	2,739	3,149	2,808	2,910	2,928	2,612	2,897	3,180	2,572	2,629	2,182
32	411.07	2,691	2,646	2,478	2,808	2,641	2,611	2,576	2,334	2,616	2,827	2,270	2,345	1,967
33	422.86	2,431	2,323	2,169	2,478	2,350	2,290	2,339	2,137	2,336	2,474	2,095	2,138	1,856
34	434.64	2,236	2,209	2,082	2,405	2,246	2,258	2,161	1,999	2,328	2,384	2,101	2,049	1,734
35	446.43	2,092	2,120	2,008	2,263	2,122	2,146	2,119	1,924	2,149	2,196	1,998	1,949	1,645
36	458.21	1,987	2,099	1,816	2,250	2,045	2,123	2,080	1,738	2,053	2,122	1,853	1,874	1,657
37	470.00	1,993	1,917	1,721	2,052	1,970	1,994	1,969	1,774	1,899	2,155	1,806	1,745	1,557
38	481.79	1,908	1,880	1,772	1,904	1,802	1,811	1,800	1,641	1,858	1,976	1,752	1,678	1,518
39	493.57	1,840	1,820	1,657	1,913	1,686	1,778	1,733	1,711	1,791	1,915	1,688	1,617	1,385
40	505.36	1,705	1,762	1,602	1,851	1,773	1,741	1,707	1,580	1,651	1,805	1,670	1,551	1,381
41	517.14	1,694	1,652	1,506	1,784	1,642	1,671	1,644	1,494	1,665	1,853	1,590	1,544	1,335
42	528.93	1,750	1,666	1,479	1,780	1,675	1,593	1,594	1,487	1,671	1,800	1,596	1,566	1,363
43	540.71	1,685	1,728	1,573	1,715	1,673	1,613	1,559	1,494	1,635	1,718	1,541	1,520	1,321
44	552.50	1,652	1,626	1,444	1,719	1,561	1,652	1,559	1,557	1,587	1,747	1,448	1,510	1,313
45	564.29	1,413	1,453	1,375	1,535	1,436	1,464	1,456	1,271	1,453	1,649	1,382	1,384	1,190
46	576.07	1,333	1,344	1,252	1,391	1,364	1,384	1,314	1,235	1,252	1,441	1,281	1,227	1,113
47	587.86	1,303	1,215	1,126	1,300	1,157	1,265	1,242	1,084	1,277	1,357	1,188	1,174	963

Table T1 (continued).

Channel	Core, section, interval (cm): / Mean energy (KeV)	195-1201D- 40R-4, 80	41R-1, 70	41R-3, 86	41R-4, 96	41R-5, 42	42R-2, 58	42R-3, 74	42R-6, 106	43R-2, 44	43R-4, 38	43R-4, 122	Empty	Water
48	599.64	1,302	1,256	1,130	1,232	1,153	1,328	1,220	1,123	1,187	1,396	1,156	1,126	997
49	611.43	1,340	1,301	1,124	1,414	1,289	1,252	1,292	1,118	1,218	1,377	1,171	1,077	962
50	623.21	1,383	1,209	1,136	1,335	1,194	1,248	1,261	1,134	1,213	1,385	1,165	1,096	923
51	635.00	1,380	1,310	1,158	1,277	1,255	1,268	1,238	1,124	1,274	1,370	1,202	1,137	933
52	646.79	1,288	1,245	1,090	1,314	1,142	1,231	1,246	1,114	1,165	1,347	1,053	1,070	841
53	658.57	1,200	1,162	1,050	1,104	1,078	1,161	1,122	1,032	1,071	1,227	1,057	970	851
54	670.36	1,052	1,062	900	1,054	963	1,077	1,017	930	975	1,138	952	939	745
55	682.14	989	889	829	975	865	913	943	856	959	972	822	910	674
56	693.93	914	898	788	964	847	849	844	723	870	921	825	783	616
57	705.71	824	785	727	884	727	830	749	771	821	867	747	663	583
58	717.50	747	718	709	770	672	713	711	655	699	713	677	530	586
59	729.29	701	640	588	738	652	644	643	609	632	754	594	510	527
60	741.07	684	662	544	679	620	668	620	582	613	687	602	482	476
61	752.86	665	653	559	697	601	610	631	571	582	692	611	472	479
62	764.64	655	626	542	677	568	610	609	507	591	664	596	482	432
63	776.43	627	637	543	641	581	583	599	469	617	720	562	468	457
64	788.21	645	596	501	682	573	625	602	526	549	715	540	455	401
65	800.00	635	620	503	650	545	623	590	512	570	670	531	441	469
66	811.79	563	606	459	666	561	580	537	521	557	618	538	418	427
67	823.57	614	556	505	591	564	595	570	493	558	610	557	433	387
68	835.36	538	589	432	570	505	546	539	499	544	621	507	394	413
69	847.14	538	537	461	567	475	548	533	467	520	610	515	382	416
70	858.93	493	523	419	604	501	529	499	427	530	612	478	377	367
71	870.71	556	484	393	557	476	538	539	472	470	542	478	367	359
72	882.50	497	522	443	554	481	536	462	395	482	570	453	325	381
73	894.29	481	566	441	586	488	508	488	415	497	580	432	381	389
74	906.07	535	500	425	571	501	531	485	439	504	584	441	374	350
75	917.86	533	523	436	585	486	528	499	454	473	575	468	399	364
76	929.64	571	545	412	562	486	564	533	415	508	657	451	329	401
77	941.43	553	494	401	556	503	524	524	454	527	622	467	341	370
78	953.21	531	512	395	592	464	577	498	431	512	604	487	317	328
79	965.00	528	526	436	609	482	512	509	403	469	618	444	379	350
80	976.79	563	508	416	542	463	475	510	422	470	546	493	368	340
81	988.57	494	522	418	565	475	487	452	410	492	542	468	306	377
82	1000.36	523	498	393	557	462	476	455	379	463	603	429	345	315
83	1012.14	499	504	391	557	426	469	451	412	475	561	404	341	314
84	1023.93	442	458	366	500	425	463	430	319	449	541	393	281	324
85	1035.71	454	410	339	469	396	416	416	366	423	475	377	252	281
86	1047.50	417	459	338	484	397	391	379	329	390	477	370	281	272
87	1059.29	428	396	330	449	414	369	366	307	355	483	351	253	310
88	1071.07	397	430	290	471	404	420	371	300	370	439	357	248	248
89	1082.86	366	417	307	468	398	398	384	332	394	457	362	279	268
90	1094.64	387	412	319	440	400	425	394	324	386	484	388	259	282
91	1106.43	394	446	367	444	389	394	388	345	350	486	377	271	257
92	1118.21	426	415	305	473	365	405	410	339	396	469	357	251	277
93	1130.00	448	431	356	423	374	407	397	331	408	491	349	258	272
94	1141.79	411	408	323	484	428	411	357	300	377	469	362	264	241
95	1153.57	433	441	320	458	345	388	371	312	420	470	357	230	241

Table T1 (continued).

Channel	Core, section, interval (cm): Mean energy (KeV)	195-1201D- 40R-4, 80	41R-1, 70	41R-3, 86	41R-4, 96	41R-5, 42	42R-2, 58	42R-3, 74	42R-6, 106	43R-2, 44	43R-4, 38	43R-4, 122	Empty	Water
96	1165.36	404	404	330	452	348	409	368	282	362	466	316	237	236
97	1177.14	315	404	276	445	383	360	399	278	342	404	313	236	232
98	1188.93	345	381	271	385	334	385	348	301	332	427	334	242	226
99	1200.71	380	350	255	409	317	354	316	271	322	359	297	227	242
100	1212.50	326	362	247	357	336	339	307	256	314	386	294	198	194
101	1224.29	287	358	240	370	327	350	308	280	305	366	291	206	220
102	1236.07	295	341	236	376	303	316	277	236	260	321	277	198	218
103	1247.86	256	286	221	341	270	311	274	255	265	315	239	181	203
104	1259.64	290	289	229	301	254	274	240	230	259	331	247	183	176
105	1271.43	275	279	208	289	259	264	238	219	298	330	239	172	187
106	1283.21	243	249	214	281	257	269	265	172	231	295	244	181	190
107	1295.00	242	251	193	262	210	225	218	161	228	269	235	158	194
108	1306.79	219	253	184	235	254	249	227	191	225	241	216	169	161
109	1318.57	231	229	183	239	240	216	214	176	230	231	226	165	184
110	1330.36	237	223	186	208	208	252	188	170	216	236	203	158	165
111	1342.14	210	232	186	228	213	246	200	196	211	248	207	189	184
112	1353.93	211	260	187	216	185	235	219	169	192	216	209	172	169
113	1365.71	242	219	189	241	222	211	220	214	208	254	223	183	166
114	1377.50	250	245	203	235	244	251	238	217	214	305	231	175	176
115	1389.29	261	251	187	300	273	275	239	220	253	354	287	191	201
116	1401.07	292	341	240	346	309	293	293	274	281	443	356	207	198
117	1412.86	382	456	281	467	412	352	403	294	337	572	393	232	225
118	1424.64	517	598	317	590	542	516	494	338	423	740	464	242	256
119	1436.43	605	736	381	903	697	663	621	396	529	932	520	261	246
120	1448.21	784	871	441	1,069	760	735	716	477	653	990	669	278	294
121	1460.00	758	899	495	1,163	837	812	750	483	717	1,069	663	269	276
122	1471.79	782	907	491	1,160	845	917	731	470	709	1,004	600	251	279
123	1483.57	673	780	466	952	693	771	689	412	622	889	491	231	221
124	1495.36	506	679	334	731	538	649	582	323	460	662	404	207	167
125	1507.14	373	493	254	469	404	463	424	223	395	493	301	163	169
126	1518.93	263	343	181	334	268	349	299	165	279	323	229	137	138
127	1530.71	197	235	161	198	205	222	182	124	201	225	176	117	131
128	1542.50	159	194	136	166	161	187	179	146	152	157	122	108	113
129	1554.29	153	134	128	124	112	152	142	98	126	152	110	115	99
130	1566.07	125	147	103	122	119	125	123	113	108	125	114	118	92
131	1577.86	137	114	92	125	112	124	132	112	133	136	121	93	117
132	1589.64	148	115	108	100	114	115	109	112	133	129	113	115	113
133	1601.43	133	108	113	100	113	124	128	129	118	126	114	101	98
134	1613.21	109	121	125	103	99	107	108	104	114	123	99	101	102
135	1625.00	109	99	105	132	109	118	101	105	136	110	129	103	96
136	1636.79	118	115	102	110	104	116	110	104	108	127	94	98	86
137	1648.57	108	113	108	106	81	117	119	92	122	98	109	105	104
138	1660.36	126	110	101	105	108	108	105	105	103	98	99	105	125
139	1672.14	104	93	106	123	84	99	98	90	123	104	83	79	104
140	1683.93	82	107	90	104	92	96	114	84	109	101	96	112	115
141	1695.71	92	109	106	90	88	119	103	110	124	120	93	93	108
142	1707.50	118	106	106	92	99	108	115	85	123	127	97	102	99
143	1719.29	104	106	113	97	111	103	114	97	115	111	99	90	109

Table T1 (continued).

Channel	Core, section, interval (cm): Mean energy (KeV)	195-1201D- 40R-4, 80	41R-1, 70	41R-3, 86	41R-4, 96	41R-5, 42	42R-2, 58	42R-3, 74	42R-6, 106	43R-2, 44	43R-4, 38	43R-4, 122	Empty	Water
144	1731.07	113	122	118	136	116	121	116	109	128	121	113	111	106
145	1742.86	131	103	93	126	113	130	115	101	103	122	105	110	86
146	1754.64	104	102	115	141	97	113	106	97	107	115	98	103	121
147	1766.43	110	103	92	95	105	98	99	108	82	124	93	90	86
148	1778.21	120	90	100	103	74	101	99	74	89	106	106	85	96
149	1790.00	92	98	95	107	80	81	89	93	107	98	95	79	79
150	1801.79	93	86	78	91	80	84	89	96	104	81	93	82	89
151	1813.57	105	104	91	71	94	80	83	91	88	81	75	81	82
152	1825.36	89	85	85	68	104	76	94	78	88	84	96	78	78
153	1837.14	100	100	90	68	72	80	95	80	92	62	77	64	68
154	1848.93	84	64	75	73	72	87	69	76	81	100	84	75	83
155	1860.71	85	82	83	68	63	83	79	77	74	85	81	63	79
156	1872.50	75	80	97	79	75	78	76	78	87	88	73	85	68
157	1884.29	91	84	84	83	72	79	69	64	72	68	70	81	57
158	1896.07	77	74	77	70	83	69	78	77	69	96	69	68	64
159	1907.86	59	61	69	86	83	68	77	73	71	89	84	65	69
160	1919.64	72	88	77	67	68	76	70	83	44	78	61	58	78
161	1931.43	73	65	72	79	70	78	76	69	69	86	59	56	62
162	1943.21	63	65	68	71	76	59	83	50	63	76	58	60	65
163	1955.00	53	71	57	69	65	66	60	77	70	58	69	55	61
164	1966.79	53	64	57	58	63	72	75	77	74	78	76	72	63
165	1978.57	72	62	66	58	71	71	77	72	54	67	71	58	73
166	1990.36	57	47	66	54	72	62	62	67	71	67	68	62	57
167	2002.14	73	57	74	74	76	60	65	66	64	73	63	57	59
168	2013.93	67	83	65	62	52	62	60	57	76	68	52	68	56
169	2025.71	71	75	88	69	65	69	71	64	67	66	65	65	67
170	2037.50	73	73	65	54	57	63	75	77	69	79	68	66	65
171	2049.29	61	68	74	70	61	68	91	59	53	77	68	59	76
172	2061.07	70	86	66	66	49	84	75	65	78	61	44	62	63
173	2072.86	72	70	85	83	67	66	73	75	72	55	50	63	57
174	2084.64	83	66	83	63	66	75	81	56	73	66	82	49	66
175	2096.43	70	77	76	78	59	67	71	60	82	68	75	57	62
176	2108.21	77	67	61	65	65	62	54	77	50	74	77	56	72
177	2120.00	75	62	52	57	77	60	75	59	69	75	55	71	68
178	2131.79	64	73	71	67	64	81	76	58	60	76	53	51	66
179	2143.57	79	54	69	63	59	68	85	69	65	80	61	67	51
180	2155.36	58	67	52	71	69	69	59	84	75	71	64	48	73
181	2167.14	66	58	55	63	59	78	58	59	66	68	61	47	53
182	2178.93	50	65	69	63	56	67	68	54	66	55	70	56	57
183	2190.71	63	57	61	72	62	70	67	63	54	69	62	57	60
184	2202.50	50	55	63	69	63	51	67	72	59	65	82	51	64
185	2214.29	61	59	63	60	56	64	58	67	52	54	65	67	68
186	2226.07	64	58	57	52	63	65	64	74	75	57	49	57	72
187	2237.86	59	54	66	58	55	55	60	53	63	56	57	57	60
188	2249.64	62	56	60	49	55	63	59	63	46	56	43	66	50
189	2261.43	50	57	66	51	60	49	59	52	49	63	47	52	59
190	2273.21	57	44	50	55	44	57	56	58	50	46	57	43	54
191	2285.00	53	59	47	51	49	46	57	49	62	50	60	43	59

Table T1 (continued).

Channel	Core, section, interval (cm): / Mean energy (KeV)	195-1201D- 40R-4, 80	41R-1, 70	41R-3, 86	41R-4, 96	41R-5, 42	42R-2, 58	42R-3, 74	42R-6, 106	43R-2, 44	43R-4, 38	43R-4, 122	Empty	Water
192	2296.79	64	53	59	49	45	49	46	50	67	54	48	60	64
193	2308.57	69	52	51	57	47	49	51	69	58	62	48	53	43
194	2320.36	62	44	60	55	53	52	52	62	56	53	50	47	64
195	2332.14	56	54	49	37	56	73	57	50	56	61	69	57	43
196	2343.93	44	43	61	41	46	55	57	69	54	53	52	57	47
197	2355.71	69	51	52	60	58	58	47	42	51	62	59	60	49
198	2367.50	45	55	43	46	41	52	53	59	48	47	49	40	49
199	2379.29	44	54	40	45	48	54	45	62	42	48	47	40	40
200	2391.07	46	56	53	53	42	58	56	60	55	47	41	44	40
201	2402.86	57	55	57	50	42	67	59	53	56	56	62	52	51
202	2414.64	60	52	54	37	35	50	53	52	44	47	40	39	48
203	2426.43	50	51	53	52	46	56	65	50	46	52	52	47	55
204	2438.21	63	59	53	42	52	58	42	46	44	64	55	50	53
205	2450.00	57	56	54	49	45	45	50	53	55	51	43	63	58
206	2461.79	49	47	54	51	54	65	41	58	51	55	62	47	59
207	2473.57	53	53	53	69	45	58	54	49	56	63	58	47	40
208	2485.36	64	67	55	54	52	55	64	61	51	58	60	55	47
209	2497.14	66	67	54	46	65	60	72	66	56	66	66	60	59
210	2508.93	59	58	69	69	57	58	50	56	60	67	64	55	47
211	2520.71	74	52	64	51	68	59	62	61	71	65	71	56	47
212	2532.50	71	58	56	53	54	63	66	75	69	70	58	62	57
213	2544.29	64	78	67	68	67	58	65	68	72	66	64	58	63
214	2556.07	79	71	51	56	76	68	81	61	63	82	50	53	58
215	2567.86	76	58	41	86	58	75	66	71	65	74	66	50	56
216	2579.64	74	55	66	69	54	58	62	78	52	72	54	68	54
217	2591.43	73	66	54	68	72	64	66	65	75	66	62	59	45
218	2603.21	66	70	55	54	66	64	61	66	50	70	65	46	65
219	2615.00	66	64	54	62	54	51	53	56	71	78	57	52	61
220	2626.79	65	67	45	59	52	56	49	56	68	70	63	52	64
221	2638.57	70	56	61	64	46	60	55	70	59	54	59	58	54
222	2650.36	59	50	50	51	54	41	53	51	47	52	42	40	53
223	2662.14	52	52	50	54	64	70	44	45	37	51	46	40	65
224	2673.93	69	53	45	49	44	43	38	65	60	71	47	41	48
225	2685.71	59	49	50	54	50	44	58	43	56	57	40	44	49
226	2697.50	49	49	46	42	41	49	42	40	56	53	43	42	41
227	2709.29	49	47	46	59	44	54	44	54	57	53	57	56	50
228	2721.07	40	49	53	37	51	55	57	58	40	58	58	45	59
229	2732.86	56	53	58	52	58	58	52	53	56	49	56	48	59
230	2744.64	52	49	49	42	53	59	57	47	47	57	62	48	47
231	2756.43	43	51	58	40	45	47	51	38	44	58	60	57	53
232	2768.21	55	69	47	52	52	50	46	50	55	53	67	35	51
233	2780.00	40	55	46	50	60	64	46	55	48	54	57	56	50
234	2791.79	38	48	53	57	48	53	44	52	62	54	48	39	47
235	2803.57	40	52	51	46	60	57	57	51	51	49	63	38	44
236	2815.36	44	30	47	41	48	53	39	45	50	55	63	45	57
237	2827.14	37	34	43	37	41	54	37	40	42	46	38	64	48
238	2838.93	45	57	49	51	58	40	64	50	47	63	50	57	54
239	2850.71	56	56	47	55	60	44	58	36	68	61	41	54	30

Table T1 (continued).

Channel	Core, section, interval (cm): / Mean energy (KeV)	195-1201D- 40R-4, 80	41R-1, 70	41R-3, 86	41R-4, 96	41R-5, 42	42R-2, 58	42R-3, 74	42R-6, 106	43R-2, 44	43R-4, 38	43R-4, 122	Empty	Water
240	2862.50	56	54	42	40	56	52	51	58	36	60	56	37	47
241	2874.29	55	66	47	54	45	59	58	53	51	48	53	46	60
242	2886.07	58	58	51	55	58	59	64	55	48	52	41	46	49
243	2897.86	46	42	57	53	52	71	53	59	58	45	49	56	51
244	2909.64	40	47	61	28	62	46	47	48	51	46	39	37	48
245	2921.43	56	40	53	44	56	55	54	56	47	54	41	48	49
246	2933.21	51	50	41	38	45	54	43	38	52	52	44	39	42
247	2945.00	34	53	44	46	41	38	39	42	61	43	42	31	38
248	2956.79	38	41	43	33	48	41	48	48	37	50	43	38	47

Note: This table is also available in **ASCII.**

Table T1 (continued).

Channel	Core, section, interval (cm): Mean energy (KeV)	195-1201D- 44R-1, 64	44R-2, 38	44R-3, 34	44R-4, 52	44R-5, 52	44R-6, 128	45R-2, 70	45R-4, 114	45R-5, 50	46R-1, 56	Empty	Water
0	33.93	0	1	1	1	1	3	1	2	0	1	5	3
1	45.71	4,503	4,524	4,545	4,606	4,627	4,568	4,281	5,299	4,945	4,409	4,413	4,110
2	57.50	3,233	3,421	3,298	3,301	3,557	3,304	3,002	4,337	3,806	3,240	2,955	2,657
3	69.29	3,095	3,501	3,242	3,263	3,437	3,222	2,871	4,620	3,768	3,114	2,648	2,470
4	81.07	3,432	3,964	3,481	3,674	4,009	3,810	3,235	5,442	4,493	3,576	2,970	2,750
5	92.86	4,205	4,751	4,335	4,372	4,924	4,478	3,758	6,763	5,428	4,356	3,329	3,489
6	104.64	4,860	5,631	5,107	5,015	6,246	5,327	4,531	8,795	7,112	4,921	3,782	3,851
7	116.43	5,790	7,011	6,039	6,060	7,561	6,173	5,270	12,201	9,270	5,733	4,113	4,346
8	128.21	5,845	7,058	6,252	6,108	7,466	6,317	5,570	10,811	8,997	6,032	4,544	4,573
9	140.00	5,712	6,681	6,175	6,149	7,283	5,861	5,601	9,652	8,119	6,341	4,699	4,447
10	151.79	6,095	7,021	6,456	6,255	7,568	6,268	5,884	9,524	7,907	6,540	5,209	4,643
11	163.57	6,905	7,549	6,794	6,709	8,169	6,699	6,547	10,232	8,545	7,124	6,012	4,860
12	175.36	6,940	7,851	7,449	7,112	8,538	7,154	6,683	10,788	9,162	7,519	6,267	5,088
13	187.14	7,358	8,003	7,439	7,237	8,759	6,967	6,858	10,895	9,272	7,846	6,610	5,096
14	198.93	7,145	8,101	7,627	7,330	8,521	7,091	6,836	10,677	9,168	7,520	6,635	4,896
15	210.71	7,046	7,873	7,429	7,020	8,516	7,027	6,676	10,395	8,885	7,516	6,609	5,005
16	222.50	7,169	7,942	7,472	7,417	8,460	7,145	6,881	10,647	9,032	7,368	6,795	4,973
17	234.29	7,129	7,927	7,254	7,121	8,179	6,931	6,698	10,543	9,097	7,347	6,918	4,896
18	246.07	6,785	7,622	7,195	7,114	8,033	6,649	6,354	10,114	8,476	7,180	6,875	4,541
19	257.86	6,642	7,326	6,758	6,609	7,592	6,468	6,103	9,983	8,386	6,801	6,279	4,593
20	269.64	6,468	7,386	6,589	6,621	7,833	6,629	6,212	11,075	8,856	6,607	6,163	4,411
21	281.43	6,107	7,277	6,555	6,263	7,719	6,360	5,705	11,426	9,140	6,224	5,376	4,152
22	293.21	5,314	6,160	5,495	5,329	6,247	5,420	4,856	8,708	7,313	5,576	4,850	3,684
23	305.00	4,616	5,246	4,883	4,827	5,416	4,815	4,252	6,942	5,979	4,753	4,349	3,311
24	316.79	4,240	4,871	4,394	4,483	4,855	4,441	3,958	6,461	5,548	4,452	4,002	3,115
25	328.57	4,170	4,512	4,173	4,302	4,726	4,313	3,825	6,161	5,246	4,158	3,785	3,028
26	340.36	3,853	4,297	3,935	4,016	4,341	3,965	3,552	5,739	4,950	3,900	3,434	2,850
27	352.14	3,494	3,901	3,543	3,596	3,954	3,688	3,244	5,393	4,435	3,518	3,213	2,579
28	363.93	3,273	3,664	3,383	3,430	3,686	3,496	3,103	5,195	4,363	3,232	3,057	2,473
29	375.71	3,255	3,722	3,327	3,395	3,756	3,494	3,162	5,411	4,331	3,231	2,988	2,402
30	387.50	3,157	3,668	3,225	3,318	3,790	3,458	2,874	5,084	4,258	3,226	2,833	2,379
31	399.29	2,935	3,311	3,095	3,039	3,306	3,030	2,651	4,469	3,862	3,074	2,629	2,182
32	411.07	2,610	2,877	2,720	2,673	2,939	2,758	2,364	3,769	3,298	2,682	2,345	1,967
33	422.86	2,361	2,599	2,430	2,392	2,552	2,523	2,215	3,344	2,914	2,405	2,138	1,856
34	434.64	2,168	2,532	2,206	2,259	2,535	2,370	2,050	3,255	2,707	2,298	2,049	1,734
35	446.43	2,127	2,367	2,178	2,215	2,306	2,200	1,975	3,115	2,644	2,113	1,949	1,645
36	458.21	2,067	2,167	2,039	2,110	2,250	2,135	1,912	3,007	2,518	2,118	1,874	1,657
37	470.00	2,011	2,211	1,979	2,031	2,110	2,131	1,809	2,812	2,425	2,035	1,745	1,557
38	481.79	1,869	2,047	1,882	1,863	2,087	2,011	1,716	2,744	2,301	1,978	1,678	1,518
39	493.57	1,779	2,071	1,813	1,824	2,004	1,816	1,660	2,628	2,303	1,741	1,617	1,385
40	505.36	1,772	1,826	1,812	1,776	1,873	1,838	1,562	2,601	2,200	1,775	1,551	1,381
41	517.14	1,662	1,891	1,732	1,756	1,930	1,875	1,495	2,461	2,140	1,719	1,544	1,335
42	528.93	1,714	1,885	1,698	1,765	1,845	1,758	1,570	2,490	2,105	1,692	1,566	1,363
43	540.71	1,672	1,858	1,640	1,741	1,894	1,706	1,469	2,510	2,159	1,630	1,520	1,321
44	552.50	1,636	1,807	1,639	1,593	1,861	1,745	1,454	2,308	1,967	1,675	1,510	1,313
45	564.29	1,499	1,651	1,601	1,495	1,632	1,591	1,346	2,183	1,919	1,530	1,384	1,190
46	576.07	1,307	1,482	1,346	1,384	1,479	1,443	1,193	2,034	1,735	1,354	1,227	1,113
47	587.86	1,309	1,413	1,275	1,265	1,388	1,332	1,120	2,002	1,616	1,270	1,174	963

Table T1 (continued).

Channel	Core, section, interval (cm): Mean energy (KeV)	195-1201D- 44R-1, 64	44R-2, 38	44R-3, 34	44R-4, 52	44R-5, 52	44R-6, 128	45R-2, 70	45R-4, 114	45R-5, 50	46R-1, 56	Empty	Water
48	599.64	1,277	1,374	1,256	1,276	1,406	1,319	1,171	2,082	1,768	1,275	1,126	997
49	611.43	1,228	1,515	1,319	1,284	1,539	1,370	1,162	2,403	1,804	1,231	1,077	962
50	623.21	1,276	1,489	1,343	1,379	1,505	1,448	1,085	2,343	1,856	1,341	1,096	923
51	635.00	1,259	1,531	1,290	1,290	1,531	1,343	1,129	2,278	1,919	1,310	1,137	933
52	646.79	1,171	1,392	1,265	1,271	1,453	1,349	1,107	1,963	1,728	1,280	1,070	841
53	658.57	1,151	1,208	1,195	1,124	1,284	1,197	997	1,731	1,532	1,147	970	851
54	670.36	1,001	1,157	1,008	1,053	1,144	1,086	892	1,591	1,344	1,107	939	745
55	682.14	982	1,052	944	916	1,040	996	795	1,391	1,225	952	910	674
56	693.93	841	989	887	920	954	930	752	1,316	1,092	937	783	616
57	705.71	778	865	819	848	989	905	635	1,189	1,039	828	663	583
58	717.50	683	803	736	802	819	749	555	1,109	985	789	530	586
59	729.29	708	782	701	715	795	751	528	1,112	909	705	510	527
60	741.07	671	757	626	691	723	782	507	1,138	968	685	482	476
61	752.86	638	765	658	632	786	715	569	1,112	936	671	472	479
62	764.64	665	775	615	655	763	691	528	1,126	921	685	482	432
63	776.43	635	741	636	647	760	683	514	1,106	920	669	468	457
64	788.21	619	678	595	642	717	675	509	1,099	895	633	455	401
65	800.00	558	662	638	598	712	709	488	1,076	858	649	441	469
66	811.79	584	675	614	651	702	666	508	983	820	599	418	427
67	823.57	559	717	594	555	647	605	457	941	832	574	433	387
68	835.36	564	621	553	574	626	616	433	993	743	575	394	413
69	847.14	516	643	558	519	608	618	474	954	771	586	382	416
70	858.93	518	582	538	576	645	593	409	967	705	563	377	367
71	870.71	521	590	494	524	642	614	402	875	783	550	367	359
72	882.50	518	576	514	594	611	540	411	933	710	568	325	381
73	894.29	510	607	489	602	612	561	414	934	745	551	381	389
74	906.07	506	617	552	535	625	589	439	1,003	781	530	374	350
75	917.86	508	673	553	517	632	596	431	1,010	806	531	399	364
76	929.64	514	672	544	552	648	629	446	1,118	846	575	329	401
77	941.43	511	671	540	585	668	649	425	1,166	863	535	341	370
78	953.21	510	650	587	549	639	605	435	1,118	805	556	317	328
79	965.00	522	629	537	570	689	558	397	1,070	853	568	379	350
80	976.79	517	625	528	551	680	629	428	1,011	855	509	368	340
81	988.57	528	580	517	554	619	573	393	1,025	792	507	306	377
82	1000.36	471	585	515	498	608	556	387	972	758	547	345	315
83	1012.14	472	580	471	475	584	560	371	914	727	515	341	314
84	1023.93	445	519	470	508	540	520	343	749	662	502	281	324
85	1035.71	399	497	444	401	482	502	321	724	584	482	252	281
86	1047.50	429	519	454	433	473	499	284	644	549	473	281	272
87	1059.29	407	424	402	457	476	465	340	648	556	423	253	310
88	1071.07	409	476	432	401	472	420	303	668	555	426	248	248
89	1082.86	406	490	389	402	433	420	320	646	578	443	279	268
90	1094.64	416	469	420	441	445	510	341	668	544	476	259	282
91	1106.43	412	488	409	452	506	473	319	664	562	513	271	257
92	1118.21	400	478	411	441	522	479	290	701	545	462	251	277
93	1130.00	363	520	450	446	518	470	313	686	530	467	258	272
94	1141.79	409	495	382	462	504	476	301	633	562	467	264	241
95	1153.57	371	491	436	426	434	429	310	651	564	471	230	241

Table T1 (continued).

Channel	Core, section, interval (cm): Mean energy (KeV)	195-1201D- 44R-1, 64	44R-2, 38	44R-3, 34	44R-4, 52	44R-5, 52	44R-6, 128	45R-2, 70	45R-4, 114	45R-5, 50	46R-1, 56	Empty	Water
96	1165.36	391	450	373	430	449	453	278	574	530	432	237	236
97	1177.14	391	463	396	398	403	427	274	632	526	456	236	232
98	1188.93	341	426	352	406	423	396	271	613	469	423	242	226
99	1200.71	334	409	341	370	408	428	244	591	467	422	227	242
100	1212.50	327	394	354	385	378	382	268	550	447	399	198	194
101	1224.29	308	386	309	371	376	371	240	528	436	386	206	220
102	1236.07	294	317	328	324	386	340	212	467	390	359	198	218
103	1247.86	271	314	307	309	331	325	233	453	437	367	181	203
104	1259.64	279	307	298	291	339	331	196	449	355	329	183	176
105	1271.43	252	302	256	284	287	292	202	382	352	287	172	187
106	1283.21	229	273	260	285	318	280	210	425	336	268	181	190
107	1295.00	241	236	258	236	278	277	191	353	321	249	158	194
108	1306.79	216	291	241	233	272	255	195	376	311	234	169	161
109	1318.57	204	233	206	264	245	267	183	350	306	258	165	184
110	1330.36	205	256	189	226	242	244	201	309	269	229	158	165
111	1342.14	214	249	235	246	246	239	209	333	283	229	189	184
112	1353.93	225	255	226	246	229	267	201	381	266	233	172	169
113	1365.71	240	244	250	246	242	268	209	401	303	242	183	166
114	1377.50	240	288	240	239	285	284	224	447	348	279	175	176
115	1389.29	269	341	266	255	299	291	256	513	363	297	191	201
116	1401.07	345	395	320	416	382	386	262	645	448	367	207	198
117	1412.86	417	515	413	475	487	531	308	816	593	480	232	225
118	1424.64	460	717	526	675	659	648	338	1,128	767	610	242	256
119	1436.43	595	900	659	807	861	893	389	1,309	889	844	261	246
120	1448.21	761	1,040	801	939	1,021	1,024	425	1,499	1,123	997	278	294
121	1460.00	831	1,177	858	974	1,124	1,142	387	1,521	1,108	1,067	269	276
122	1471.79	875	1,076	866	911	1,066	1,038	397	1,476	1,140	1,097	251	279
123	1483.57	651	961	736	848	901	953	334	1,217	1,014	1,005	231	221
124	1495.36	575	694	593	662	655	694	303	1,003	787	779	207	167
125	1507.14	399	497	430	486	489	500	211	675	624	616	163	169
126	1518.93	287	342	311	337	292	352	165	439	433	393	137	138
127	1530.71	256	228	211	241	232	229	145	313	298	257	117	131
128	1542.50	165	173	174	179	161	178	142	264	214	195	108	113
129	1554.29	153	139	144	132	162	142	128	206	198	140	115	99
130	1566.07	110	146	108	110	147	122	102	200	175	119	118	92
131	1577.86	122	107	127	112	146	129	114	182	164	120	93	117
132	1589.64	117	151	130	133	124	126	104	194	172	106	115	113
133	1601.43	124	119	118	107	140	127	103	175	156	88	101	98
134	1613.21	119	137	114	121	161	123	112	199	147	93	101	102
135	1625.00	109	130	126	129	132	119	101	194	180	93	103	96
136	1636.79	113	109	104	116	128	135	131	177	152	108	98	86
137	1648.57	116	130	119	92	113	111	117	161	122	106	105	104
138	1660.36	117	117	134	110	117	93	118	153	143	88	105	125
139	1672.14	102	105	113	113	113	97	108	165	129	107	79	104
140	1683.93	110	121	96	109	117	98	110	132	144	109	112	115
141	1695.71	100	111	105	94	113	99	106	152	141	100	93	108
142	1707.50	124	107	123	119	110	103	91	156	161	96	102	99
143	1719.29	121	130	121	111	125	133	102	160	154	97	90	109

Table T1 (continued).

Channel	Core, section, interval (cm): Mean energy (KeV)	195-1201D- 44R-1, 64	44R-2, 38	44R-3, 34	44R-4, 52	44R-5, 52	44R-6, 128	45R-2, 70	45R-4, 114	45R-5, 50	46R-1, 56	Empty	Water
144	1731.07	120	95	115	109	136	115	104	200	157	102	111	106
145	1742.86	98	108	133	106	107	117	112	172	157	121	110	86
146	1754.64	97	111	100	108	108	118	110	168	145	83	103	121
147	1766.43	102	117	100	78	111	117	107	175	125	89	90	86
148	1778.21	106	113	91	106	127	90	109	154	133	116	85	96
149	1790.00	97	95	109	93	99	118	99	154	145	94	79	79
150	1801.79	95	105	99	98	124	100	81	142	112	109	82	89
151	1813.57	88	89	101	92	92	95	70	131	113	74	81	82
152	1825.36	94	103	91	85	89	79	87	114	98	84	78	78
153	1837.14	93	98	74	73	96	96	78	121	92	87	64	68
154	1848.93	95	86	80	90	87	77	87	119	99	83	75	83
155	1860.71	62	100	88	79	81	75	75	107	113	93	63	79
156	1872.50	74	80	84	79	84	79	74	109	114	65	85	68
157	1884.29	84	87	79	77	87	78	69	111	100	61	81	57
158	1896.07	69	86	69	71	88	73	88	100	83	74	68	64
159	1907.86	74	93	68	82	71	69	69	103	71	67	65	69
160	1919.64	74	82	82	68	73	75	69	117	86	77	58	78
161	1931.43	77	67	62	65	67	79	67	103	86	57	56	62
162	1943.21	80	71	83	77	74	76	69	102	78	60	60	65
163	1955.00	63	77	70	77	62	49	77	112	83	49	55	61
164	1966.79	55	78	63	72	75	77	64	92	78	68	72	63
165	1978.57	79	68	70	71	75	83	65	91	74	48	58	73
166	1990.36	65	65	73	54	74	70	57	93	78	53	62	57
167	2002.14	73	78	79	65	64	68	62	98	73	74	57	59
168	2013.93	81	59	75	74	81	81	70	83	85	71	68	56
169	2025.71	52	82	70	74	69	63	55	108	83	63	65	67
170	2037.50	73	68	86	73	69	63	62	109	91	75	66	65
171	2049.29	68	89	65	64	70	74	60	120	102	66	59	76
172	2061.07	69	69	82	55	68	65	66	118	89	79	62	63
173	2072.86	66	69	76	56	84	92	57	126	89	69	63	57
174	2084.64	72	87	70	72	83	72	49	109	85	74	49	66
175	2096.43	71	73	80	64	84	64	62	126	93	74	57	62
176	2108.21	60	80	73	93	81	82	73	117	103	54	56	72
177	2120.00	64	82	95	73	73	60	65	122	95	72	71	68
178	2131.79	62	67	85	65	77	64	56	106	102	68	51	66
179	2143.57	69	83	59	69	88	66	46	114	107	70	67	51
180	2155.36	52	64	70	66	74	65	60	112	97	65	48	73
181	2167.14	56	66	73	63	76	71	58	91	96	66	47	53
182	2178.93	58	59	80	66	62	70	62	83	85	59	56	57
183	2190.71	67	63	80	68	76	76	61	81	77	47	57	60
184	2202.50	66	73	56	69	63	47	56	114	81	68	51	64
185	2214.29	54	78	58	78	74	49	60	126	84	73	67	68
186	2226.07	51	67	59	46	62	72	72	101	76	59	57	72
187	2237.86	65	75	58	58	75	65	56	97	99	60	57	60
188	2249.64	47	66	59	70	58	80	50	102	92	56	66	50
189	2261.43	55	60	49	45	59	62	62	94	77	51	52	59
190	2273.21	70	59	64	50	52	50	44	90	70	49	43	54
191	2285.00	70	61	56	61	55	61	52	84	69	50	43	59

Table T1 (continued).

Channel	Core, section, interval (cm): Mean energy (KeV)	195-1201D- 44R-1, 64	44R-2, 38	44R-3, 34	44R-4, 52	44R-5, 52	44R-6, 128	45R-2, 70	45R-4, 114	45R-5, 50	46R-1, 56	Empty	Water
192	2296.79	58	50	58	46	56	48	65	104	88	60	60	64
193	2308.57	66	61	49	45	68	53	45	95	76	58	53	43
194	2320.36	44	67	57	63	64	66	64	79	66	52	47	64
195	2332.14	69	67	58	47	61	50	45	72	66	59	57	43
196	2343.93	58	47	51	40	66	49	40	69	50	49	57	47
197	2355.71	44	54	57	57	57	40	48	74	64	52	60	49
198	2367.50	55	59	48	56	65	54	50	67	80	44	40	49
199	2379.29	56	26	49	61	48	48	47	66	65	61	40	40
200	2391.07	54	54	72	45	48	54	49	71	59	49	44	40
201	2402.86	69	58	50	56	44	47	57	73	65	53	52	51
202	2414.64	50	49	53	56	53	46	60	68	71	52	39	48
203	2426.43	45	54	60	44	62	49	50	69	70	50	47	55
204	2438.21	50	40	67	51	60	50	50	68	67	52	50	53
205	2450.00	47	49	67	53	51	64	53	71	70	55	63	58
206	2461.79	59	56	65	52	56	83	48	98	67	53	47	59
207	2473.57	43	73	49	58	50	69	55	111	67	56	47	40
208	2485.36	46	73	54	60	57	46	58	101	82	51	55	47
209	2497.14	63	62	53	53	78	81	55	116	81	57	60	59
210	2508.93	63	64	47	68	58	56	66	135	104	58	55	47
211	2520.71	68	70	60	63	76	59	71	110	110	52	56	47
212	2532.50	67	69	65	55	76	70	65	127	106	50	62	57
213	2544.29	72	88	94	70	83	77	59	158	140	62	58	63
214	2556.07	71	89	74	77	90	79	69	141	96	66	53	58
215	2567.86	74	78	74	75	75	81	69	132	117	70	50	56
216	2579.64	61	72	71	74	95	72	65	126	109	74	68	54
217	2591.43	56	78	69	52	80	77	61	129	105	80	59	45
218	2603.21	70	78	65	74	82	62	83	113	113	75	46	65
219	2615.00	69	77	58	63	63	61	64	102	97	53	52	61
220	2626.79	51	66	54	46	69	60	64	98	75	60	52	64
221	2638.57	53	56	56	53	66	49	64	81	60	35	58	54
222	2650.36	58	59	57	60	53	53	32	77	76	44	40	53
223	2662.14	41	61	53	28	47	46	65	61	85	55	40	65
224	2673.93	62	63	58	41	61	50	44	50	73	58	41	48
225	2685.71	43	55	32	48	46	45	50	57	68	44	44	49
226	2697.50	38	48	55	45	47	56	45	57	51	55	42	41
227	2709.29	43	55	57	52	46	44	45	66	57	51	56	50
228	2721.07	52	49	60	49	47	49	47	57	69	51	45	59
229	2732.86	59	57	43	45	66	57	57	60	65	43	48	59
230	2744.64	34	57	44	51	59	45	52	74	56	50	48	47
231	2756.43	49	41	52	58	45	55	60	61	61	44	57	53
232	2768.21	44	54	51	53	51	52	46	59	43	44	35	51
233	2780.00	35	48	60	38	65	48	49	60	50	45	56	50
234	2791.79	50	55	50	44	44	45	59	56	60	58	39	47
235	2803.57	57	50	42	46	69	54	55	72	39	46	38	44
236	2815.36	52	59	40	48	43	54	60	62	65	58	45	57
237	2827.14	56	45	36	46	53	53	53	65	47	44	64	48
238	2838.93	54	44	58	42	39	48	50	47	58	48	57	54
239	2850.71	43	56	37	47	55	44	46	49	69	52	54	30

Table T1 (continued).

Channel	Core, section, interval (cm): / Mean energy (KeV)	195-1201D- 44R-1, 64	44R-2, 38	44R-3, 34	44R-4, 52	44R-5, 52	44R-6, 128	45R-2, 70	45R-4, 114	45R-5, 50	46R-1, 56	Empty	Water
240	2862.50	48	54	48	48	39	38	54	64	68	33	37	47
241	2874.29	57	61	58	38	56	54	56	51	55	66	46	60
242	2886.07	43	49	52	47	42	59	46	47	52	40	46	49
243	2897.86	45	60	50	57	62	48	40	62	58	39	56	51
244	2909.64	45	42	42	58	46	53	43	47	57	46	37	48
245	2921.43	43	55	52	55	50	46	39	49	46	62	48	49
246	2933.21	55	39	49	41	44	44	45	44	51	56	39	42
247	2945.00	58	45	36	37	39	34	38	52	42	52	31	38
248	2956.79	46	37	39	48	32	50	38	51	48	38	38	47

Table T2. Calibration results for the NGR during Leg 195.

Calibration standard	Peak energy (KeV)	Energy window
^{40}K	1460	121
^{208}Tl	2615	219

Table T3. Concentrations of K_2O, U, and Th calculated from NGR measurements taken over a 4-hr counting period.

Depth (mbsf)	K_2O (wt%)	U (ppm)	Th (ppm)
460.41	1.34	1.02	5.44
465.60	1.70	0.97	5.16
468.54	0.88	0.71	3.87
470.09	1.99	1.72	9.02
471.05	1.51	0.83	4.46
476.58	1.54	1.00	5.34
478.24	1.43	0.89	4.78
482.98	0.88	0.74	3.99
485.93	1.24	0.88	4.72
488.54	1.94	1.36	7.16
489.38	1.17	0.61	3.35
494.34	1.51	0.95	5.09
495.78	1.98	1.41	7.45
497.04	1.57	1.07	5.68
498.72	1.77	1.07	5.68
500.22	1.84	1.55	8.13
502.48	1.93	1.12	5.97
505.50	0.82	0.65	3.56
508.50	2.74	2.95	15.29
509.36	2.06	2.06	10.76
513.46	2.01	1.10	5.86